Structural Biology and Molecular Biophysics

Structural and Dynamic Impacts of Single-atom Disruptions to Guide RNA Interactions within the Recognition Lobe of *Geobacillus stearothermophilus* Cas9

Reviewed Preprint
v2 • March 27, 2025
Revised by authors

Reviewed Preprint
v1 • July 16, 2024

Helen B Belato, Alexa L Knight, Alexandra M D'Ordine, Chinmai Pindi, Zhiqiang Fan, Jinping Luo, Giulia Palermo, Gerwald Jogl, George P Lisi

Department of Molecular Biology, Cell Biology & Biochemistry, Brown University, Providence, United States • Departments of Bioengineering and Chemistry, University of California Riverside, Riverside, United States • Brown University RNA Center, Providence, United States

eLife Assessment

This study offers **valuable** insights into the conformational dynamics of the nucleic acid recognition lobe of GeoCas9, a thermophilic Cas9 from Geobacillus stearothermophilus. The authors investigate the influence of local dynamics and allosteric regulation on guide RNA binding affinity and DNA cleavage specificity through advanced NMR techniques and mutagenesis. The revised manuscript incorporates new experimental data, including molecular dynamics simulations and additional RNA binding studies, which provide **convincing** support for the findings. While the mutations studied do not lead to significant changes in GeoCas9 cleavage activity, the study contributes to a better understanding of the allosteric mechanisms and interdomain communication in Cas9 enzymes, and will be of great interest to biochemists and biophysicists exploring these complex systems.

https://doi.org/10.7554/eLife.99275.2.sa4

Abstract

The intuitive manipulation of specific amino acids to alter the activity or specificity of CRISPR-Cas9 has been a topic of great interest. As a large multi-domain RNA-guided endonuclease, the intricate molecular crosstalk within the Cas9 protein hinges on its conformational dynamics, but a comprehensive understanding of the extent and timescale of the motions that drive its allosteric function and association with nucleic acids remains elusive. Here, we investigated the structure and multi-timescale molecular motions of the recognition (Rec) lobe of *Geo*Cas9, a thermophilic Cas9 from *Geobacillus stearothermophilus*. Our results provide new atomic details about the *Geo*Rec subdomains (*Geo*Rec1, *Geo*Rec2) and the full-length domain in solution. Two rationally designed mutants, K267E and R332A, enhanced and redistributed micro-millisecond flexibility throughout *Geo*Rec, and NMR

studies of the interaction between *Geo*Rec and its guide RNA showed that mutations reduced this affinity and the stability of the ribonucleoprotein complex.

Despite measured biophysical differences due to the mutations, DNA cleavage assays reveal no functional differences in on-target activity, and similar specificity. These data suggest that guide RNA interactions can be tuned at the biophysical level in the absence of major functional losses, but also raise questions about the underlying mechanism of *Geo*Cas9, since analogous single-point mutations have significantly impacted on- and off-target DNA editing in mesophilic *S. pyogenes* Cas9. A K267E/R332A double mutant did also did not enhance *Geo*Cas9 specificity, highlighting the robust tolerance of mutations to the Rec lobe of *Geo*Cas9 and species-dependent complexity of Rec across Cas9 paralogs. Ultimately, this work provides an avenue by which to modulate the structure, motion, and guide RNA interactions at the level of the Rec lobe of *Geo*Cas9, setting the stage for future studies of *Geo*Cas9 variants and their effect on its allosteric mechanism.

Introduction

The vast majority of Cas systems explored as genome editors originate from mesophilic hosts. The emergence of the thermophilic *Geo*Cas9, with DNA cleavage function up to 85°C, can expand CRISPR technology to higher temperature regimes and stabilities,[1,2] but its regulatory mechanism relative to canonical Cas9s must be established. The *Sp*Cas9, which originates from the mesophilic *Streptococcus pyogenes*, as well as *Geo*Cas9, are both effectors of Type-II CRISPR systems. Interestingly, the Type II-A *Sp*Cas9 has been by far the most used Cas enzyme, including in ongoing clinical trials.[3,4] But Cas9 homologs of the Type II-C class, such as *Neisseria meningitis* (*Nme*Cas9) and *Campylobacter jejuni* (*Cje*Cas9), to which *Geo*Cas9 belongs, have been validated for mammalian genome editing,[2,5,6] reinforcing the need to better understand this CRISPR class.

The similar domain arrangements of *Geo*Cas9 and *Sp*Cas9 led us to initially speculate that these could share atomic level mechanistic similarities.[7] *Geo*Cas9 utilizes a guide RNA (gRNA) to localize and unwind a double-stranded DNA (dsDNA) target after recognition of its 5'NNNNCRAA-3' protospacer adjacent motif (PAM).[2,8] Upon recognition of the PAM sequence by the PAM-Interacting domain (PI), Cas9-bound guide (gRNA) forms an RNA:DNA hybrid with the target DNA strand. Initially thought to be part of the PI domain[2], the wedge (WED) domain recognizes the repeat:anti-repeat region of the gRNA and the dsDNA upstream of the target region.[9] The Rec lobe of Cas9 is responsible for orienting the RNA:DNA hybrid, as well as the adjacent nuclease domains, into their active conformations.[10–13] Coordinated cleavage of the target and non-target DNA strand then occurs via the HNH and RuvC nucleases, respectively. The *Geo*Cas9 nuclease active sites within HNH and RuvC are spatially distinct from the PAM recognition site in the PI domain, necessitating structural and dynamic changes that allosterically couple dsDNA binding to cleavage. Biochemical[11,14,15] and structural[16,17] experiments using the extensively studied *Sp*Cas9 have revealed that its function is governed by a sophisticated allosteric mechanism that transfers gRNA and dsDNA binding information from the Rec lobe to the distal catalytic sites. A dynamically driven allosteric signal spans the HNH domain of *Sp*Cas9, enabled by the plasticity of the Rec lobe, which orchestrates the conformational activation required for DNA cleavage.[14,18] Our prior work revealed a divergence in the timescales of allosteric motions in the *Sp*Cas9 and *Geo*Cas9 HNH domains[7,17] suggesting an unusually flexible HNH and unique allosteric mode of regulation for *Geo*Cas9. It is therefore also possible that docking of the gRNA with *Geo*Cas9, and thus its interaction with the RNA:DNA hybrid, may differ from the *Sp*Cas9 system, as *Geo*Cas9 contains a truncated Rec lobe with only two of the three canonical subdomains.

The high thermal stability and more compact size of *Geo*Cas9 (it is 281 residues shorter than *Sp*Cas9) can be especially important for *in vivo* delivery applications, since promising viral vectors (*i.e.* adeno-associated virus, AAV) have cargo capacities of ~4.7kb,[19] which prevents *Sp*Cas9-gRNA packaging into a single AAV vector but permits "all-in-one" delivery of *Geo*Cas9-sgRNA.[12] Until the very recent cryo-EM structures of *Geo*Cas9,[20,21] little was known about specific residues that influence its structure, gRNA binding, or function. Our recent NMR work with *Sp*Cas9 uncovered pathways of micro-millisecond timescale motions that propagate chemical information related to allostery and specificity through *Sp*Rec and its RNA:DNA hybrid,[16,17] prompting us to investigate this phenomenon in *Geo*Rec.

An atomic-level structural understanding of specificity in large multi-domain protein-nucleic acid complexes like Cas9 is often difficult to address by NMR spectroscopy. Although dynamic ensembles in DNA repair enzymes have provided some insight,[22] many efforts to improve Cas9 specificity and reduce off-target activity have relied on large mutational screens[23] or error-prone PCR[24], which are less intuitive. Inter-subunit allosteric communication between the catalytic HNH domain and the Rec lobe is critical to Cas9 specificity, as the binding of off-target DNA sequences at Rec alter HNH dynamics to affect DNA cleavage.[8,25,26] To further probe the fundamental role of protein motions in the function and specificity of *Geo*Cas9, as well as the effect of protein-nucleic acid interactions on its structural signatures, we engineered two mutations in *Geo*Rec (K267E and R332A, housed within *Geo*Rec2). We hypothesized that these variants could enhance *Geo*Cas9 specificity (*i.e.* limit its off-target cleavage) for two reasons. First, the chosen mutation sites are homologous to those of specificity-enhancing variants of *Sp*Cas9.[24,27] Second, altered Cas9-gRNA interactions have been shown to be a consequence of specificity-enhancement and these charged residues appear to directly interact with the gRNA.[10,11,15,28] Balancing these two points is the fact that Type-II Cas systems generally have conserved nuclease domains, but are delineated by highly varied Rec lobes.[12] This implies that the structural and dynamic properties of Rec may play an outsized role in differentiating the functions of *Sp*Cas9 and *Geo*Cas9, which may not be identical. Nevertheless, our work provides new insight into the biophysical, biochemical, and functional role of the *Geo*Rec lobe and how mutations modulate the domain itself and its interaction with gRNA in full-length *Geo*Cas9.

Results

The structural similarity of GeoRec1, GeoRec2, and GeoRec facilitates NMR analysis of protein dynamics and RNA affinity

*Geo*Cas9 is a 1087 amino acid polypeptide, thus we employed a "divide and concur" approach for NMR studies, which we previously showed to be useful for quantifying allosteric structure and motion in *Sp*Cas9.[16,17,29,30] The *Geo*Rec lobe is comprised of subdomains *Geo*Rec1 and *Geo*Rec2, which likely work together to recognize nucleic acids. We engineered constructs of the *Geo*Rec1 (136 residues, 16 kDa) and *Geo*Rec2 (212 residues, 25 kDa) subdomains and solved the X-ray crystal structure of *Geo*Rec2 at 1.49 Å, which aligns remarkably well with the structure of the *Geo*Rec2 domain within the AlphaFold model (RMSD 1.03 Å) and new cryo-EM structure of *Geo*Cas9 (RMSD 1.10 Å, **Figure 1A**). We were neither able to crystallize *Geo*Rec1 nor full-length *Geo*Cas9 in the apo state, but our *Geo*Rec2 crystal structure represents the structure of the subdomain within the full-length *Geo*Cas9 protein quite well. Our previous studies of *Geo*HNH also show identical superpositions of X-ray crystal structures with full-length Cas complexes.[7] In addition to the individual subdomains, we also generated an NMR construct of the intact *Geo*Rec (370 residues, 43 kDa).

Despite only 22% sequence identity, the structure of *Sp*Rec3 and *Geo*Rec2 are highly similar (RMSD 2.00 Å, Figure S1). The structure of *Geo*Rec1, in contrast, does not align perfectly with *Sp*Rec1, instead, it partially aligns with both *Sp*Rec1 and *Sp*Rec2 (Figure S1). Thus, the nearly identical

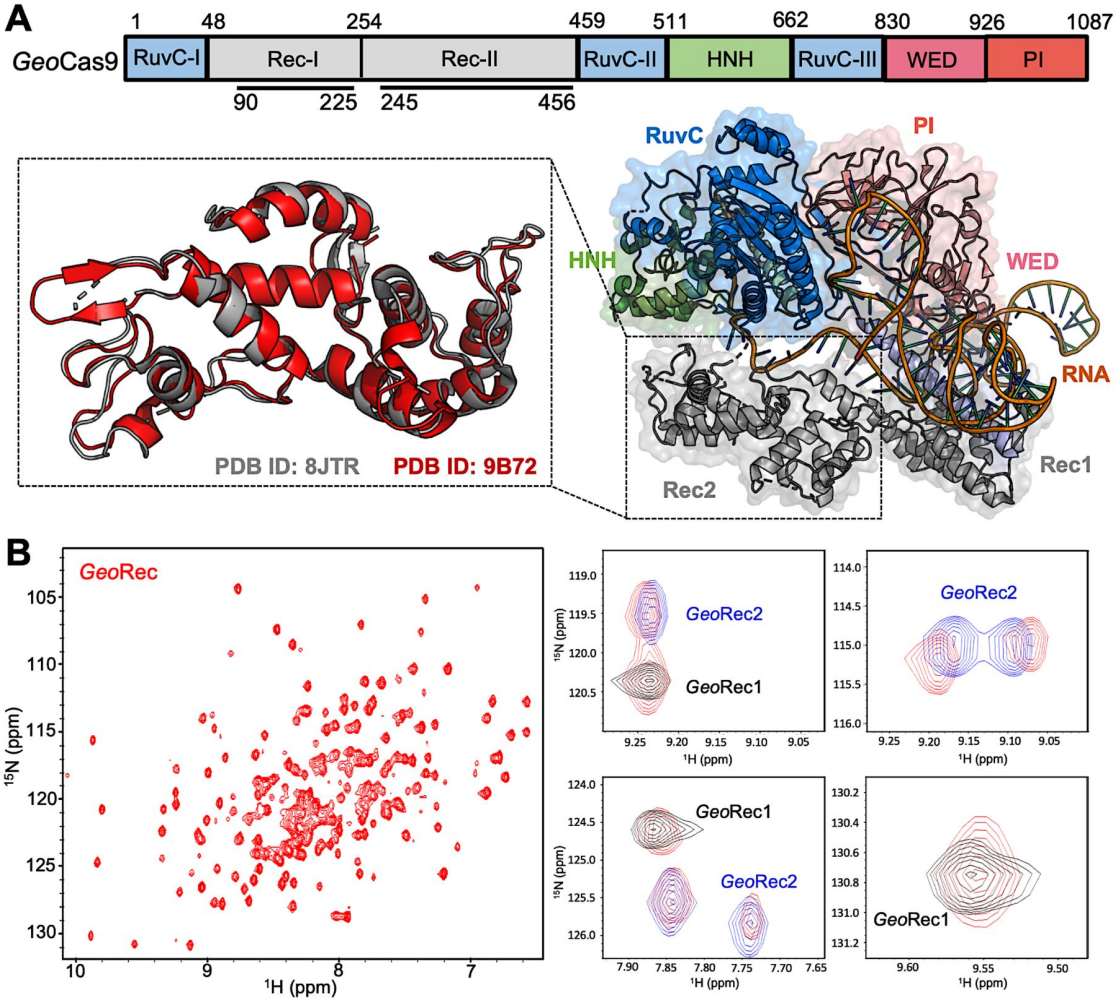

Figure 1.

(A) Arrangement of *Geo*Cas9 domains across the primary sequence. The cryo-EM structure of *Geo*Cas9 in complex with gRNA (PDB: 8JTR) shows poor resolution of HNH. The *Geo*Rec2 domain from PDB: 8JTR (gray) is overlaid with our X-ray structure of *Geo*Rec2 (red, PDB: 9B72). **(B)** 1H15N TROSY HSQC NMR spectrum of *Geo*Rec collected at 850 MHz. Overlays of this spectrum with resonances from spectra of *Geo*Rec1 (black) and *Geo*Rec2 (blue) demonstrate a structural similarity between the isolated subdomains and intact *Geo*Rec.

*Sp*Rec3 and *Geo*Rec2 architectures and their intrinsic dynamics may be a common thread among Type II Cas9s of different size and PAM preference. To capture atomic-level signatures of *Geo*Rec, we obtained well-resolved ^{1}H-^{15}N NMR fingerprint spectra for all three protein constructs and assigned the amide backbones (Figure S2). ^{1}H-^{15}N amide and ^{1}H-$^{13}CH_3$ Ile, Leu, and Val (ILV)-methyl NMR spectra (**Figure 1B**, **S3**) of *Geo*Rec overlay very well with those of its individual subdomains, suggesting that the linkage of subdomains within the full-length *Geo*Rec polypeptide does not alter their individual folds. Consistent with this observation, circular dichroism (CD) thermal unfolding profiles of *Geo*Rec1 (T_m ~ 34 °C) and *Geo*Rec2 (T_m = 61.50°C) are distinct and occur as separate events in the unfolding profile of *Geo*Rec (**Figure S4**). The dumbbell shape of *Geo*Rec, with its two globular subdomains connected by a short flexible linker, is a likely contributor to these biophysical properties.

Rationally designed GeoRec2 mutants do not substantially impact the GeoRec structure

To understand how the structure and gRNA interactions of *Geo*Cas9 can be modulated at the level of *Geo*Rec, we engineered two charge-altering point mutants in the *Geo*Rec2 subdomain, K267E and R332A. Based on the AlphaFold2 model of *Geo*Cas9, both of these residues are < 5Å from the bound RNA:DNA hybrid and were predicted to interface with the nucleic acids directly (**Figure 2A/B**). A new experimental cryo-EM structure of *Geo*Cas9 confirmed the interaction between K267 and the gRNA, but does not report a < 5Å interaction of R332 with the gRNA.[31] The rationale for our designed mutations was also that removal of positive charge would weaken the interactions between *Geo*Cas9 and the gRNA, affecting K_d via the electrostatics or dynamics of the *Geo*Rec lobe. Studies of *Sp*Cas9 revealed that interaction of *Sp*Rec3 (analogous to *Geo*Rec2) with its RNA:DNA hybrid triggers conformational rearrangements that allow the catalytic HNH domain to sample its active conformation.[11] Thus, *Sp*Rec3 acts as an allosteric effector that recognizes the RNA:DNA hybrid to activate HNH. Mismatches (*i.e.* off-target DNA sequences) in the target DNA generally prevent *Sp*Rec3 from undergoing the full extent of its required conformational rearrangements, leaving HNH in a “proofreading” state with its catalytic residues too far from the DNA cleavage site. Off-target DNA cleavage by Cas9 remains an area of intense study and substantial effort from various groups has gone into mitigating such effects.[15,23,28,32,33] Indeed, many high-specificity *Sp*Cas9 variants contain mutations within *Sp*Rec3 that increase the threshold for its conformational activation, reducing the propensity for HNH to sample its active state in the presence of off-target DNA sequences.[11,15,23] Studies of flexibility within Rec itself, as well as its gRNA interactions in the presence of mutations, are therefore essential to connecting biophysical properties to function and specificity in related Cas9s.

The K267E *Geo*Rec2 variant is sequentially and structurally similar to a specificity enhancing site in *Sp*Cas9 (K526E), within the evoCas9 system.[27] The *Sp*Cas9 K526E mutation substantially reduced off-target activity alone, but was even more effective in conjunction with three other single-point mutations in *Sp*Rec3.[27] The R332A *Geo*Rec2 variant also resembles one mutation within a high-specificity *Sp*Cas9 variant, an early iteration of HiFi *Sp*Cas9 called HiFi Cas9-R691A.[24] We assessed mutation-induced changes to local structure in *Geo*Rec via NMR chemical shift perturbations in ^{1}H-^{15}N HSQC backbone amide spectra. Consistent with experiments using *Geo*Rec2 alone, chemical shift perturbations and line broadening are highly localized to the mutation sites. (**Figure 2C-F**). Perturbation profiles of the *Geo*Rec2 subdomain and intact *Geo*Rec also implicate the same residues as sensitive to the mutations (**Figure S5**).

CD spectroscopy revealed that wild-type (WT), K267E, and R332A *Geo*Rec2 maintained similar alpha-helical secondary structure, though the thermostability of both variants was slightly reduced from that of WT *Geo*Rec2 (**Figure S6**). The T_m of WT *Geo*Rec2 is ~62 °C, consistent with the T_m of the full-length *Geo*Cas9, while that of K267E *Geo*Rec2 was decreased to ~55 °C. Though the R332A *Geo*Rec2 T_m remains ~62 °C, this variant underwent a smaller unfolding event near 40

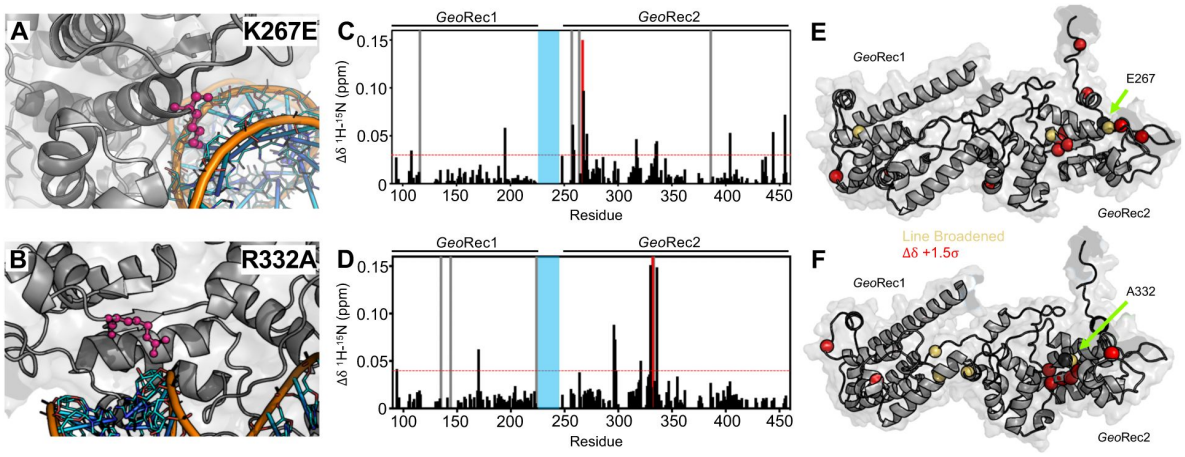

Figure 2.

(A, B) Sites of selected mutations within *Geo*Rec2, K267 and R332, are highlighted as purple sticks directly facing the RNA and DNA modeled from *Nme*Cas9 (PDB ID: 6JDV), allowing for prediction of the binding orientation within *Geo*Cas9. NMR chemical shift perturbations caused by the K267E **(C)** or R332A (**D**) mutations are plotted for each residue of *Geo*Rec. Gray bars denote sites of line broadening, the blue bar denotes an unassigned region of *Geo*Rec corresponding to the native Rec1-Rec2 linker, and the red bar indicates the mutation site. The red dashed line indicates 1.5α above the 10% trimmed mean of the data. Chemical shift perturbations 1.5α above the 10% trimmed mean are mapped onto K267E **(E)** and R332A **(F)** *Geo*Rec (red spheres). Resonances that have broadened beyond detection are mapped as yellow spheres and the mutation sites are indicated by a black sphere and green arrow.

°C before completely unfolding. These data suggest that despite small structural perturbations, both mutations are destabilizing to *Geo*Rec2, which led us to expect a change in NMR-detectable protein dynamics.

Mutations enhance and redistribute molecular motions within GeoRec2

Due to the high molecular weight of the intact *Geo*Rec lobe, decays in NMR signal associated with spin relaxation experiments were significant and hampered data quality. Thus, we focused on quantifying the molecular motions of the *Geo*Rec2 subdomain, where the K267E and R332A mutations reside, and the chemical shift perturbations are most apparent. To obtain high-quality per-residue information representative of *Geo*Rec, we measured longitudinal (R_1) and transverse (R_2) relaxation rates and heteronuclear ^{1}H-[^{15}N] NOEs (**Figure S7**), then used these data in a Model-free analysis of per-residue order parameters (S^2). Previous measurements of S^2 across the adjacent *Geo*HNH nuclease revealed substantial ps-ns timescale flexibility,[7] leading us to wonder whether a similar observation would be made for *Geo*Rec2, which abuts *Geo*HNH. Such a finding could suggest that HNH-Rec2 crosstalk in *Geo*Cas9 is driven primarily by rapid bond vector fluctuations. However, unlike *Geo*HNH, S^2 values for *Geo*Rec2 are globally elevated, suggesting that the ps-ns motions of this subdomain arise primarily from global tumbling of the protein in solution. We therefore carried out Carr-Purcell-Meiboom-Gill (CPMG) relaxation dispersion NMR experiments to assess the flexibility of *Geo*Rec2 on slower timescales, which has been linked to chemical information transfer in the well-studied *Sp*Cas9.[10,16,17,29] Evidence of µs-ms motions (*i.e.* curved relaxation dispersion profiles) is observed in 17 residues within the *Geo*Rec2 core, spanning its interfaces to Rec1 and HNH (**Figure 3B**). Such motions are completely absent from *Geo*HNH, thus two neighboring domains, *Geo*Rec2 and *Geo*HNH, diverge in their intrinsic flexibility (at least in isolation), raising questions about the functional implications of these motions in *Geo*Rec2. We previously showed that heightened flexibility of *Sp*Rec3 via specificity-enhancing mutations concomitantly narrowed the conformational space sampled by *Sp*HNH, highlighting a “motional trade-off” between the domains. Manipulation of the flexibility of *Sp*Cas9 and *Geo*Cas9 domains by mutagenesis also impacts aspects of nucleic acid binding and cleavage,[1,10,14,15,29] which led us to investigate similar perturbations in *Geo*Rec2.

Since *Sp*Rec3 and *Geo*Rec2 have similar structures and µs-ms flexibility, we speculated that charge-altering mutations would modulate the biophysical properties of *Geo*Rec and the function of *Geo*Cas9, as observed for *Sp*Cas9. We investigated K267E and R332A *Geo*Rec2 with NMR spin relaxation, as described for WT *Geo*Rec2 (*vide supra*). An analysis of chemical exchange rates, k_{ex}, derived from dual-field CPMG relaxation dispersion show a global k_{ex} for WT *Geo*Rec2 of 147 ± 41 s^{-1}. The K267E mutation, which directly contacts the nucleic acids, shifts the globally fitted k_{ex} to 376 ± 89 s^{-1}, while the R332A variant maintains a global k_{ex} similar to that of WT *Geo*Rec2 (142 ± 28 s^{-1}) and consistent with its similar thermal stability. The global fit of the K267E variant is based on CPMG profiles of 33 residues, while that of R332A is derived from 18 residues (Table S1). Interestingly, the residues participating in the global motions of both variants are distinct from those of WT *Geo*Rec2, demonstrating that residue-specific flexibility is redistributed throughout *Geo*Rec2, which suggests an altered intradomain molecular crosstalk within the larger *Geo*Rec. Indeed, perturbation to NMR-detectable motions in *Sp*Cas9 rewired its allosteric signaling and enzymatic function.[16,29] A similar dynamic modulation of *Geo*Cas9 may fine-tune its DNA cleavage, which has been demonstrated within the *Geo*HNH nuclease[1] and wedge (WED) domains.[32] We also assessed the ps-ns fluctuations of *Geo*Rec2 variants (a negligible contribution to the WT *Geo*Rec2 dynamic profile) and calculated order parameters from R_1, R_2 and ^{1}H-[^{15}N] NOE relaxation measurements (**Figure 3C**). Bond vector fluctuations on the ps-ns timescale are only locally altered, thus the mutation-induced reshuffling of these motions is negligible ($\langle \Delta S^2 \rangle \leq 0.1$) and suggests that, like WT *Geo*Rec2, ps-ns motion arises primarily from global tumbling in solution.

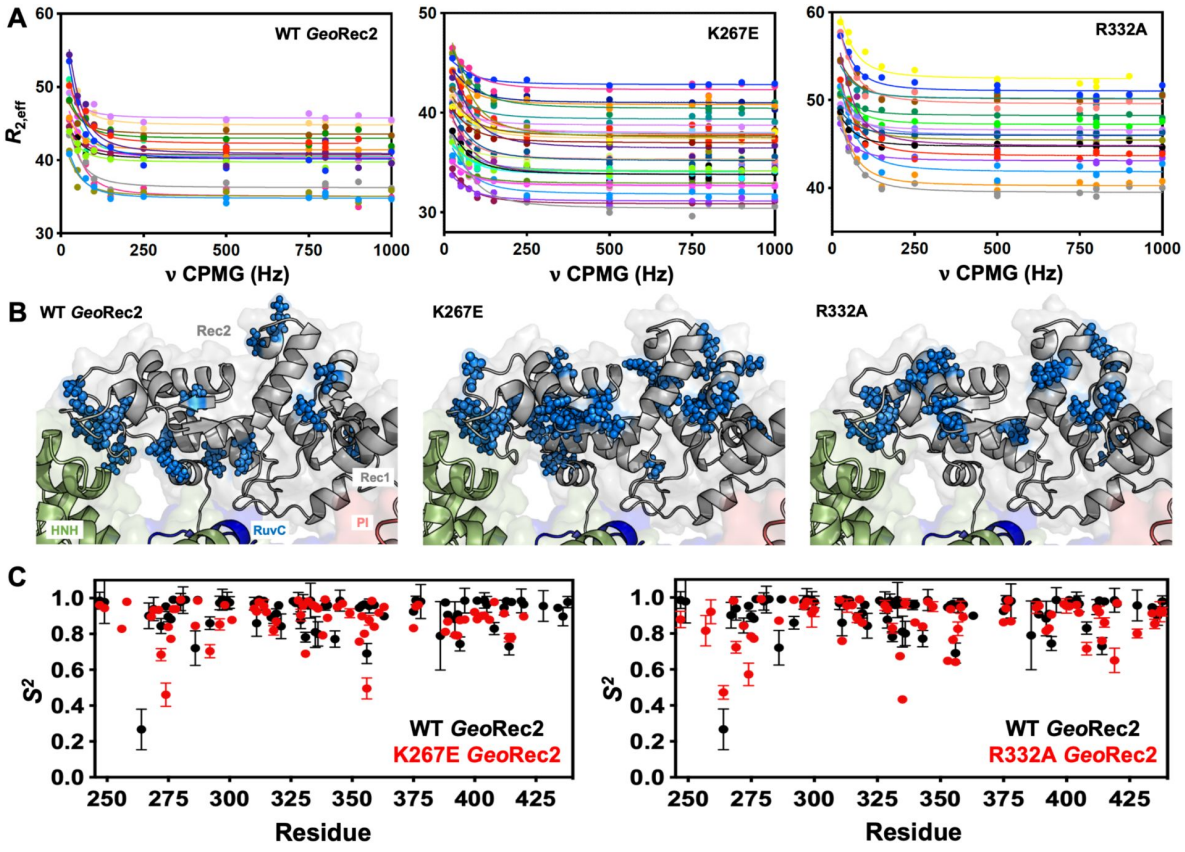

Figure 3.

(A) CPMG relaxation dispersion profiles of all residues with evidence of µs-ms motion, fit to a global *k*ex of 147 ± 41 s^{-1} (WT *Geo*Rec2, left), 376 ± 89 s^{-1} (K267E *Geo*Rec2, center), and 142 ± 28 s^{-1} (R332A *Geo*Rec2, right) collected at 25 °C and 600 MHz. Residues are colored in accordance with Table S1. Relaxation dispersion profiles for individual resonances are shown in Figures S8-S10. **(B)** Sites exhibiting CPMG relaxation dispersion in **(A)** are mapped to *Geo*Rec as blue spheres. Adjacent domains within the cryo-EM structure of *Geo*Cas9 are also shown. **(C)** Per-residue NMR order parameters of WT (black), K267E, and R332A (red, separate plots) *Geo*Rec.

Mutations within GeoRec alter its affinity for guide RNA

The role of the Rec lobe in orienting the RNA:DNA hybrid within Cas9 is crucial to its function.[10–13] Thus, the structure, motions, and nucleic acid interactions of Rec represent a critical piece of the Cas9 signaling machinery. Previous studies of *Sp*Cas9 revealed that gRNA binding to the Rec lobe induces a global structural rearrangement of the protein that positions the adjacent HNH into its "proofreading" state,[15] after which target DNA binding positions the nucleases into active conformations for cleavage.[15,34] We wondered if the atomistic details of the apo *Geo*Cas9-to-RNP transition could be captured by NMR using the *Geo*Rec construct. In our previous studies, we used an *in vitro* DNA cleavage assay with *Geo*Cas9 and a 141nt gRNA containing a 21nt spacer targeting the mouse *Tnnt2* gene locus.[1] Since this assay was already established, we utilized the same gRNA sequence. However, truncating this gRNA was necessary to optimize binding studies for NMR analysis. We focused on the 5' end of the gRNA, which includes the spacer sequence, based on the *Geo*Cas9 AlphaFold2 model and structural data from *Nme*Cas9 and *Sp*Cas9 showing interactions between the Rec lobe and this region of the gRNA. The subsequent cryo-EM structure of *Geo*Cas9 corroborated this interaction.[20] Initial attempts using a truncated 101nt gRNA resulted in poor NMR spectra. An overlay of the ^{1}H-^{15}N HSQC NMR spectra of apo *Geo*Rec and *Geo*Rec-RNP at a 1:1 molar ratio showed extensive line broadening (Figure S11), likely due to the large size of the complex (75.5 kDa). To mitigate this issue, a 39nt gRNA containing the 21bp spacer sequence was selected for its ability to maintain the NMR signal while being long enough to interact fully with the Rec lobe, as suggested by prior structures. When bound to *Geo*Rec, this complex is 55.6 kDa and a ^{1}H-^{15}N NMR spectral overlay of apo *Geo*Rec and the domain bound to 39nt gRNA shows clear, resolved resonances with significant chemical shift perturbations and line broadening (**Figure 4A/B**, **S11**). The strongest chemical shift perturbations are localized to the *Geo*Rec2 subdomain that interfaces with the RNA:DNA hybrid at the PAM distal end, where previous studies of specificity-enhancing variants of *Sp*Cas9 have identified alterations in nucleic acid binding to *Sp*Rec3.[16] It is not known whether specific residues at the PAM distal binding interface of *Geo*Rec2 play a similar role. Line broadening is evident in both *Geo*Rec1 and *Geo*Rec2, primarily localized to the RNA:DNA hybrid interface revealed in recent *Geo*Cas9 structures. Microscale thermophoresis (MST) experiments quantified the affinity of *Geo*Rec for gRNA, producing a K_d = 3.3 ± 1.5 μM that is consistent with the concentration-dependent NMR chemical shift perturbations (**Figure 5A**).

To understand how the K267E and R332A mutants impact gRNA binding to *Geo*Rec, we conducted gRNA titration experiments via NMR and observed that chemical shift perturbations were attenuated in both variants, relative to WT *Geo*Rec. Despite this muted structural effect, the impact from gRNA-induced line broadening remains substantial in the *Geo*Rec1 subdomain. Our NMR data revealed that a three-fold greater concentration of gRNA was required to induce the maximal structural and dynamic effects in the variants than is required for WT *Geo*Rec (**Figure 4A/C**), suggesting that the variants have a reduced gRNA affinity. MST experiments showed statistically significant reductions in gRNA affinity for the K267E and R332A constructs, relative to WT *Geo*Rec, where K267E *Geo*Rec produced a K_d = 7.2 ± 1.0 μM and R332A *Geo*Rec produced a K_d = 7.2 ± 1.5 μM (**Figure 5B**). The ~3-fold decrease in K_d may also be due, in part, to a change in the binding mode of the gRNA, such as a faster k_{off}. Collectively, these data reveal that mutations within *Geo*Rec primarily alter its structure around the mutation site with weaker distal effects, but more significantly impact protein dynamics and in turn, the gRNA interaction. NMR experiments also demonstrate that the presence of gRNA impacts both subdomains of *Geo*Rec, providing a significant structural interface for additional molecular tuning of nucleic acid binding.

To investigate the impact of gRNA binding on *Geo*Rec2 in greater detail, we conducted NMR titration experiments using the isolated domain, which yielded even clearer NMR spectra. **Figure S12** shows NMR spectra of WT, K267E, and R332A *Geo*Rec2 overlaid with their corresponding gRNA-bound spectra (39nt Tnnt2 RNA). At protein:RNA molar ratios used for full-length *Geo*Rec studies, the WT *Geo*Rec2 spectrum exhibited significant line broadening across the *Geo*Rec2

Figure 4.

(A) NMR chemical shift perturbations caused by gRNA binding to WT, K267E, and R332A *Geo*Rec. Gray bars denote sites of line broadening, and the blue bar denotes an unassigned region of *Geo*Rec corresponding to the flexible Rec1-Rec2 linker. The red dashed line indicates 1.5α above the 10% trimmed mean of the data. **(B)** Representative NMR resonance shifts caused by titration of 39nt gRNA into WT *Geo*Rec. **(C)** NMR titration of 39nt gRNA into K267E (top) and R332A (bottom) *Geo*Rec. The left panel of each pair demonstrates that minimal change in NMR chemical shift or resonance intensity is apparent at gRNA concentrations mimicking the WT titration. The right panel of each pair depicts the titration over a three-fold wider concentration range of gRNA, where shifts and line broadening are visible. Representative resonances are colored by increasing gRNA concentration in the legend.

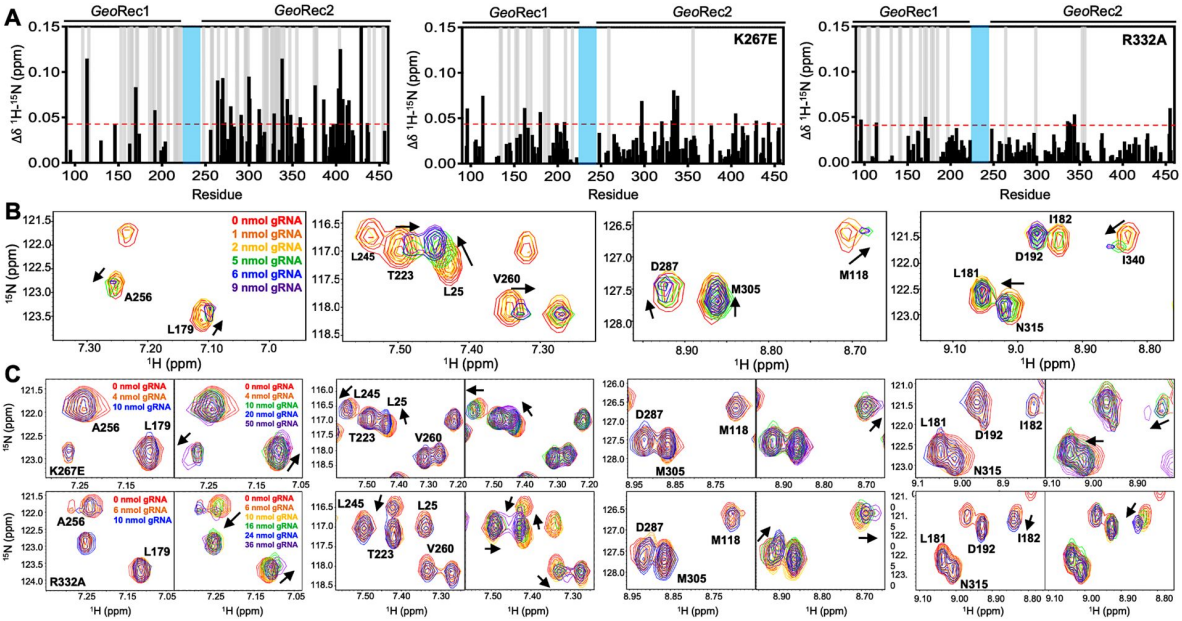

Figure 5.

Representative MST-derived profiles of WT **(A)**, K267E, and R332A **(B)** *Geo*Rec binding to a Cy5-labeled 39nt gRNA, yielding *Kd* = 3.3 ± 1.5 μM, *Kd* = 7.2 ± 1.0 μM and *Kd* = 7.2 ± 1.5 μM, respectively. Bar graphs comparing *Kd* values across n ≥ 3 replicate samples are shown for Tnnt2 gRNA **(C)** and 8UZA gRNA from a recent cryo-EM structure **(D)**. **p* < 0.05, ***p* < 0.004

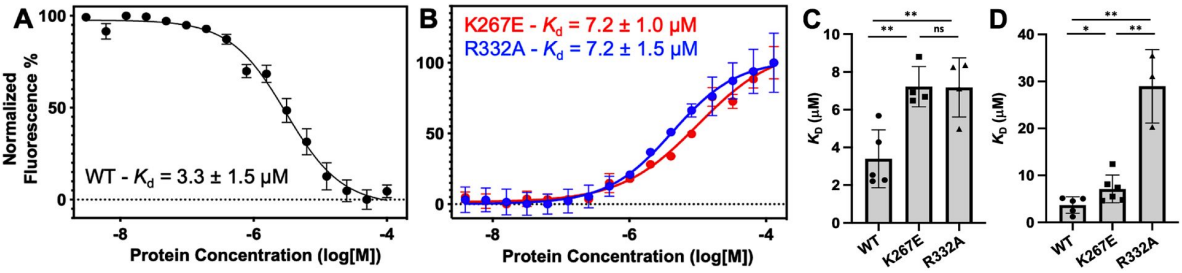

sequence. Plots of NMR peak intensities (I_{bound}/I_{free}) show substantial resonance intensity losses (**Figure S12**), with many residues likely in the intermediate exchange regime, in addition to the assumed changes in rotational correlation of the domain. In comparison, spectra of the gRNA-bound K267E and R332A *Geo*Rec2 variants showed less pronounced signal decay at the same levels of titrant, retaining nearly double the I_{bound}/I_{free} ratio across these spectra (**Figure S12**). These data are consistent with the results of NMR experiments with the 43 kDa *Geo*Rec, supporting the premise that *Geo*Rec2 mutations weaken its interaction with gRNA. The less crowded NMR spectrum of isolated *Geo*Rec2 facilitated the resolution of distinct structural features that explain the impact of the mutations on gRNA binding (**Figure S9**). For example, residue I53 adopts a similar conformation in gRNA-bound WT and K267E *Geo*Rec2 but assumes a different structural state in R332A. Conversely, residue R25 populates a WT-like structure in gRNA-bound R332A *Geo*Rec2, unlike K267E. Additionally, two resonances are observed for residue K71 in the gRNA-bound R332A NMR spectrum, indicating real-time equilibration between two structural states. This effect is unique to the R332A variant and underscores subtle structural and dynamic changes to *Geo*Rec during gRNA binding.

We further examined the NMR data to attempt to identify residues most critical for gRNA binding to *Geo*Rec. In an overlay of the WT and mutant gRNA-induced chemical shift perturbations (Δδ, **Figure S13**), it became clear that the effect of gRNA binding to *Geo*Rec variants was muted, where even at saturating concentrations, the chemical shift perturbations across the K267E and R332A *Geo*Rec2 sequences were weaker than those of same residues in WT *Geo*Rec. The residual Δδ (WT - mutant) was plotted (**Figure S13**), where positive values indicate that residues in a *Geo*Rec variant are weakly affected by gRNA, relative to WT. Negative residual Δδ denote sites where *Geo*Rec variants experience a greater structural impact from gRNA than corresponding sites in WT. Of particular interest are the positive residuals that hint at the sites in *Geo*Rec most critical for tight gRNA binding. These residues were mapped onto the *Geo*Rec structure (**Figure S13**) and termed allosteric hotspots, as many are not at the RNA interface. Mutations of these hotspots in future studies offers a potential means of precisely tuning the affinity of *Geo*Rec to gRNA. Notably, residues with positive residual Δδ (suggested as critical for tight RNA binding) largely overlap in the analysis of both variants. Specifically, residues F170, R192, H264, R269, L270, L279, H300, D301, E368, D376, D403, E405, E408, and I429 appear as allosteric hotspots (with CPMG relaxation dispersion) critical to WT-like gRNA interaction.

Having observed a reduced affinity of *Geo*Rec variants for gRNA by NMR and MST, we next quantified the impact of the K267E and R332A mutations on RNP formation and stability in full-length *Geo*Cas9. The thermal unfolding midpoint of full-length WT *Geo*Cas9 determined by CD is ~60 °C and the K267E and R332A mutations do not change the T_m of the apo protein (**Figure S14**). Upon formation of an RNP, the T_m of WT *Geo*Cas9 increases to 73°C. K267E *Geo*Cas9 retains a similar T_m increase to 70 °C, while R332A *Geo*Cas9 forms a less stable RNP with T_m of 61 °C. The trend of these data is consistent with NMR and MST, which highlight that although K267E and R332A mutations within *Geo*Rec have somewhat muted structural effects, these changes alter protein dynamics and the interaction with gRNA.

Mutations in full-length GeoCas9 alter its structural dynamics and interaction with gRNA

To further investigate the effects of mutations on protein dynamics, we performed molecular dynamics (MD) simulations based on the cryo-EM structure of full-length *Geo*Cas9 (PDB: 8UZA) in complex with gRNA and target DNA. We simulated the full-length WT *Geo*Cas9 and its K267E and R332A mutants as well as a double mutant combining K267E and R332A (**Figure 6A**), in three replicates of approximately 2 μs each. Multi-microsecond simulations revealed substantial changes in the dynamics of the GeoCas9 mutants compared to the WT (**Figure S15**). Specifically, we observed that mutations in the REC domain significantly altered the dynamics of both the Rec and the adjacent HNH (**Figure S15**). Differential root-mean-square fluctuations (ΔRMSF)

analysis of protein residues between the WT and variants further highlighted these alterations, showing increased dynamics in the HNH and Rec domains induced by the mutations (**Figure 6B**). To quantify the impact of these mutations, we analyzed protein-RNA interactions by calculating the number of contacts between *Geo*Cas9 and gRNA in the WT and mutant systems. A contact was defined as a distance between two atoms of ≤ 4.5 Å. The number of contacts was significantly reduced in all variants compared to the WT, with the most pronounced reduction observed in the K267E variant (**Figure 6C**). We next quantified gRNA-Rec domain binding by calculating the binding free energy using the MM-GBSA method over ~200 ns of stable simulation trajectories (details in Materials and Methods). Consistent with a reduction in gRNA contacts, variants with the K267E mutation exhibited a substantial reduction in binding free energy (>60 kcal mol^{-1}.) relative to the WT, whereas the R332A variant displayed a smaller reduction (<20 kcal mol^{-1}., **Figure 6D**). Notably, protein-DNA interactions remained largely unaffected, suggesting that these mutations do not impair *Geo*Cas9 DNA cleavage ability.

Additionally, we simulated a novel variant, i*Geo*Cas9 (PDB: 8UZB), containing mutations in the Rec1 and WED domains (**Figure 6A**, mutations highlighted in lime green). This variant was recently demonstrated to have enhanced specificity in genome-editing.[21] Intriguingly, i*Geo*Cas9 exhibited increased dynamics in the HNH and Rec domains, along with a reduction in gRNA binding free energy similar to the K267E and R332A mutants. These results suggest a distinct allosteric pathway involving additional residues that enables i*Geo*Cas9 to maintain improved DNA cleavage activity despite reduced gRNA binding affinity. In fact, i*Geo*Cas9 samples the greatest conformational space of any variant tested (Figure S15), suggesting a high level of flexibility is critical to enhanced specificity in *Geo*Cas9. Collectively, our simulations reveal that mutations K267E and R332A destabilize the *Geo*Cas9 interaction with gRNA, consistent with NMR observations. Furthermore, the enhanced dynamics and altered binding affinities observed in i*Geo*Cas9 indicate potential allosteric mechanisms that optimize its genome-editing functionality, where K267E and R332A evoke a similar, but lesser degree of biophysical change.

DNA cleavage assays suggest the highly stable GeoCas9 is resistant to functional changes by K267E or R332A mutations

The dynamic impact of the *Geo*Rec mutations and their altered gRNA interactions at the biophysical level led us to speculate that either mutation incorporated into full-length *Geo*Cas9 would also alter its DNA cleavage function, especially at elevated temperatures where WT *Geo*Cas9 is most active. Temperature-dependent functional alterations were previously observed for single-point mutations within *Geo*HNH.[1] Although the K267E and R332A mutations slightly diminished on-target DNA cleavage by *Geo*Cas9, the effect was very subtle and these overall cleavage activities followed the temperature dependence of WT *Geo*Cas9 quite closely (Figure S16).

To assess the impact of the K267E and R332A mutations on *Geo*Cas9 specificity, we assayed the propensity for off-target cleavage using DNA substrates with mismatches 5-6 or 19-20 base pairs from the PAM site (Figure S17, Table S2). As a control for on- and off-target activity, we assayed WT *Sp*Cas9 alongside the widely used high-specificity HiFi-*Sp*Cas9 variant[24] (Figure S17, Table S3) and found a lower percent of digested off-target (mismatched) DNA sequences when compared to WT *Sp*Cas9. As expected, WT *Geo*Cas9 was increasingly sensitive to mismatched target sequences closer to the seed site, which has been demonstrated with *Sp*Cas9 and other Cas systems.[2,6,8,35] No significant differences in activity were observed with digestion durations ranging from 1-60 minutes,[2] implying that a 1-minute digestion is sufficient for *in vitro* activity of *Geo*Cas9 with the target DNA template. While these findings generally align with prior investigations of off-target DNA cleavage,[2,6,8] there are nuanced differences. Specifically, a previous study reported ~10% cleavage of off-target DNA with a mismatch 5-6 base pairs from the PAM by WT *Geo*Cas9.[2] Our results showed nearly 50% cleavage for the same off-target mismatch, but still a significant decrease in cleavage from on-target or 19-20 base pair distal mismatches. This could be due to the relatively high RNP concentrations (600-900 nM) in our assay

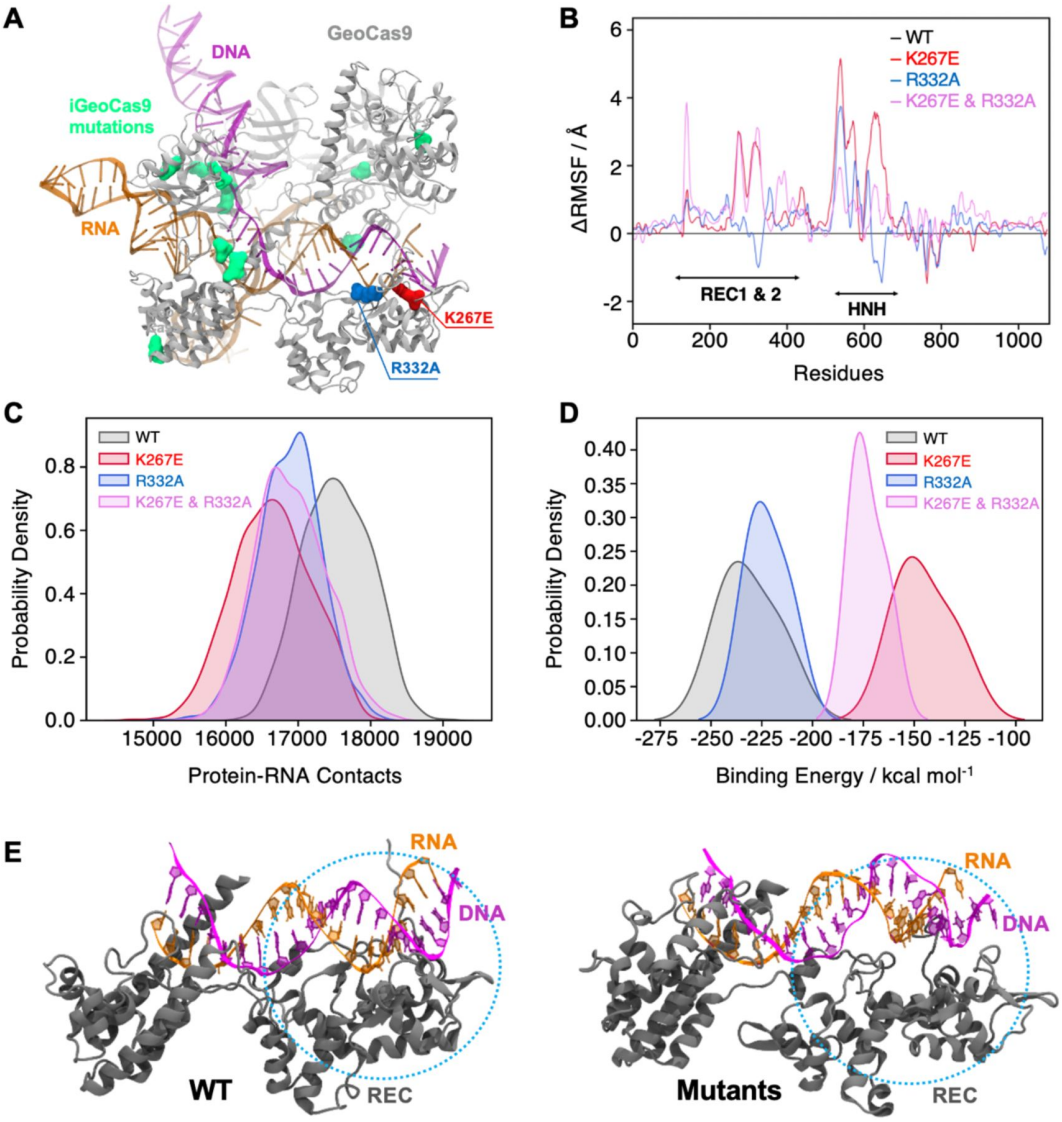

Figure 6

Effects of mutations in full-length *Geo*Cas9 revealed by MD simulations. **(A)** The structure of *Geo*Cas9 (PDB: 8UZA, protein in gray) bound to gRNA (orange) and DNA (magenta) is shown. Mutations studied include K267E (red), R332A (blue), and the 10 mutations of i*Geo*Cas9 (lime green), all highlighted in surface representation. **(B)** Differential root-mean-square fluctuations (ΔRMSF) of protein residues computed between WT *Geo*Cas9 and the K267E (red), R332A (blue), and double mutant (pink). **(C)** Distribution of protein-RNA contacts for WT and *Geo*Cas9 variants computed over the 6 μs simulation ensemble. **(D)** Comparison of gRNA binding free energy to the Rec domain in WT *Geo*Cas9 and variants. **(E)** Representative snapshots from MD simulations illustrating structural changes in Rec-gRNA association in WT *Geo*Cas9 (left) and variants (right).

(for clear visibility on the gel), compared to prior studies with RNP concentrations σ; 500 nM.[2] Our results corresponded closely to those of prior studies with a 19-20 base pair mismatch, where off-target cleavage is tolerated by WT *Geo*Cas9.[2] Single-point mutants K267E and R332A *Geo*Cas9 have negligible impact on *Geo*Cas9 specificity (both variants follow the trend of WT *Geo*Cas9, Figure S17), which contrasts prior work with *Sp*Cas9 that demonstrated robust specificity enhancement with single-point mutations in Rec.[24,27] Additionally, a *Geo*Cas9 double mutant K267E/R332A exhibits decreased on-target cleavage efficiency, which has been noted in high-specificity Cas systems.[15,23,24,27,36–38] However, the additive effect of the K267E/R332A double mutant still does not enhance *Geo*Cas9 specificity in our assay. MST-derived binding affinities using full-length Tnnt2 gRNA and full-length WT, K267E, or R332A *Geo*Cas9 indicate that all three proteins have similar affinities for the gRNA used in the functional assays (**Figure 7**). Thus, mutations do not substantially alter full-length *Geo*Cas9 binding to Tnnt2 gRNA, supporting similar cleavage activities for these proteins. We repeated the MST experiments using a different gRNA sequence derived from the new cryo-EM structure of *Geo*Cas9 (PDB:8UZA), which has a different spacer sequence. We observed a similar trend, as all *Geo*Cas9 variants exhibited comparable affinities for this gRNA. Our functional studies illustrate an apparent resilience of *Geo*Cas9 to major functional changes at the level of Rec, despite comparable mutations having profound functional impacts in mesophilic Cas9s.

Discussion

CRISPR-Cas9 is a powerful tool for targeted genome editing with high efficiency and modular specificity.[2,15,24,27] Allosteric signals propagate DNA binding information to the HNH and RuvC nuclease domains, facilitating their concerted cleavage of double-stranded DNA.[8,10,14,15] The intrinsic flexibility of the nucleic acid recognition lobe plays a critical role in this information transfer, exerting a measure of conformational control over catalysis.[10] This study provides new insights into the structural, dynamic, and functional role of the thermophilic *Geo*Cas9 recognition lobe. Novel constructs of subdomains *Geo*Rec1 and *Geo*Rec2, as well as intact *Geo*Rec show a high structural similarity to the domains in full-length *Geo*Cas9, facilitating solution NMR experiments that captured the intrinsic allosteric motions across *Geo*Rec2. These studies revealed the existence of μs-ms timescale motions that are classically associated with allosteric signaling and enzyme function, which span the entire *Geo*Rec2 domain to its interfaces with *Geo*Rec1 and the adjacent *Geo*HNH domain.

Based on homology to specificity-enhancing variants of the better studied *Sp*Cas9, the biophysical and biochemical consequences of two mutations were tested in *Geo*Rec2, the larger *Geo*Rec lobe, and full-length *Geo*Cas9. We speculated that removing positively charged residues with potential to interact with negatively charged nucleic acids could disrupt *Geo*Cas9-gRNA complex formation, stability, and subsequent function by altering the protein or nucleic acid motions. Indeed, CPMG relaxation dispersion experiments revealed that mutations enhanced and reorganized the μs-ms flexibility of *Geo*Rec2. Further, NMR titrations showed the affinity of K267E and R332A *Geo*Rec for gRNA to be weaker than that of WT *Geo*Rec, consistent with MST-derived K_d values using the isolated domain. The mutations also diminished the stability of the full-length *Geo*Cas9 RNP complex.

The collective changes to protein dynamics, gRNA binding, and RNP thermostability suggested that mutations could modulate *Geo*Cas9 function, as observed in similar studies of *Sp*Cas9 reporting that gRNA dynamics, affecting the potential for the RNA:DNA hybrid to dissociate, have affected function.[11,15,39] Yet, the functional impact of single-point and double mutations in this work were negligible, despite homologous K-to-E and R-to-A single point mutations enhancing specificity of the mesophilic *Sp*Cas9. The biophysical impact of mutations within *Geo*Rec2 and *Geo*Rec may be tempered by its evolutionary resilience and the highly stable neighboring domains in the context

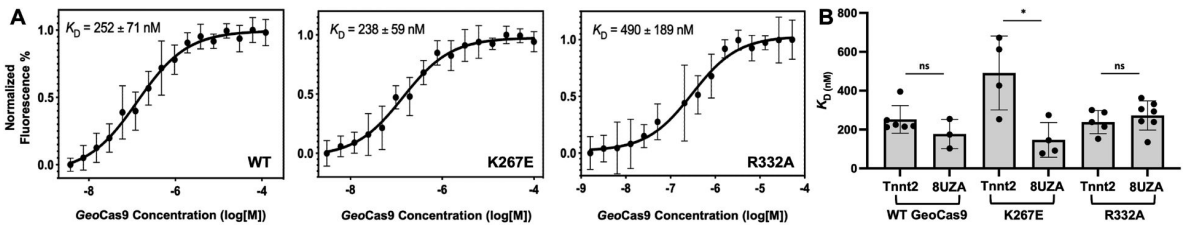

Figure 7.

(A) Representative MST-derived profiles of WT, K267E, and R332A *Geo*Cas9 binding to a Cy5-labeled full-length Tnnt2 gRNA. **(B)** Bar graph comparing *Kd* values across n ≥ 3 replicate samples are shown for Tnnt2 and 8UZA gRNA from a recent cryo-EM structure of *Geo*Cas9. *p < 0.01

of full-length *Geo*Cas9, reflected in an unchanged affinity for target DNA once the RNP was formed.[40,41] Thus, a greater number of additive (or synergistic) mutations within *Geo*Rec would be required to fine-tune activity or specificity to a large degree.

It should be noted that the effects of these and other *Geo*Rec mutations may vary *in vivo* or with alternative target cleavage sites and cell types. Such studies will be the subject of future work, as will biochemical assays of homologous mutations across diverse Cas9s, which have contributed to the wide use of CRISPR technology.[42] We also note that despite the homology between *Geo*Rec2 and *Sp*Rec3 and the latter's role in evo- and HiFi-*Sp*Cas9 variants that inspired the K267E and R332A mutations, the maximally enhanced *Sp*Cas9 variants contain four mutations each. Presumably each individual substitution plays a small role modulating specificity. However, there is no consistent pattern that discerns whether multiple mutations will have additive or synergistic impacts on Cas9 function. NMR and MD studies of high-specificity *Sp*Cas9 variants (HF-1, Hypa, and Evo, each with distinct mutations in the *Sp*Rec3 domain) reveal universal structural and dynamic variations in regions of *Sp*Rec3 that interface with the RNA;DNA hybrid.[16] Notably, a recently published variant, i*Geo*Cas9,[32] demonstrated enhanced genome-editing capabilities in HEK293T cells with eight mutations, though none in the Rec2 subdomain. This study highlighted the functional adaptability of i*Geo*Cas9 under low magnesium conditions, a trait beneficial in mammalian cells, distinguishing it from WT *Geo*Cas9. These very recently published data, as well as the findings reported here still advance our molecular understanding of the functional handles in *Geo*Cas9, relevant to the design of new enhanced variants.

This study marks the first phase of mapping allosteric motions and pathways of information flow in the *Geo*Rec lobe with solution NMR experiments. Such information transfer is critical to the crosstalk between Rec and HNH in several Cas9s. Despite NMR advancements in perdeuteration,[43] transverse relaxation-optimized spectroscopy (TROSY),[44] and sparse isotopic labeling,[45] per-residue dynamics underlying allosteric signaling in large multi-domain proteins such as *Geo*Cas9 (~126 kDa) have remained challenging to characterize. Novel cryo-EM structures of *Geo*Cas9[32] will facilitate the merging of future NMR and MD simulation studies to report on RNP dynamics and atomic level networks of communication. The identification of additional (or synergistic) allosteric hotspots within *Geo*Rec using an integrated workflow will help to further resolve the balance between structural flexibility and the unusually high stability of *Geo*Cas9, leading to new insight into targeted manipulation of RNA affinity and enhanced variants.

Here, we set out to biophysically characterize the Rec lobe of *Geo*Cas9 to obtain new understanding of its function (in the context of well-studied mesophilic Cas9s). Using an AlphaFold2 model, and later a cryo-EM structure of *Geo*Cas9, we introduced mutations based on proximal gRNA interactions and homology to specificity-enhancing sites in *Sp*Cas9. However, the mutations did not affect *Geo*Cas9 function as expected, highlighting the complicated interplay between the biophysics of mesophilic and thermophilic Cas enzymes and the difficulty of applying universal functional predictions to Cas9. The very recent report of the i*Geo*Cas9 variant further reinforces this point.[21] While high-specificity *Sp*Cas9 variants are heavily mutated in Rec3 (analogous to *Geo*Rec2), i*Geo*Cas9 lacks mutations in Rec2 entirely, raising new questions about the functional role of *Geo*Rec. MD simulations of WT *Geo*Cas9, i*Geo*Cas9, and the Rec variants revealed that while K267E and R332A induce dynamic effects on a similar trajectory to i*Geo*Cas9, a true high-specificity variant samples a very wide conformational space with displacements of both Rec and HNH (**Figures 6** and **S15**). Through further study of the fundamental mechanism of *Geo*Cas9, it remains possible that engineering of *Geo*Rec may produce high-specificity variants.

Materials and methods

Expression and purification of *Geo*Rec1, *Geo*Rec2, *Geo*Rec, and *Geo*Cas9

The *Geo*Rec1 (residues 90-225) and *Geo*Rec2 (residues 245-456) subdomains, as well as the entire *Geo*Rec lobe (residues 90-456) of *G. stearothermophilus* Cas9 were engineered into a pET28a vector with a N-terminal His_6-tag and a TEV protease cleavage site. The K267E and R332A mutations were separately introduced into the *Geo*Rec2 plasmid. Plasmids were transformed into BL21 (DE3) cells (New England Biolabs). Protein samples for CD spectroscopy, MST, and functional assays were grown in Lysogeny Broth (LB, Fisher), while isotopically labeled samples for NMR were grown in M9 minimal media (deuterated for *Geo*Rec2 and *Geo*Rec) containing $CaCl_2$, $MgSO_4$, MEM vitamins, and 1.0 g/L ^{15}N ammonium chloride and 2.0 g/L ^{13}C glucose (Cambridge Isotope Laboratories), as the sole nitrogen and carbon sources, respectively. Cells were induced with 1 mM IPTG after reaching an OD_{600} of 0.8–1.0 and grown for 4 hours at 37 °C post induction. The cells were harvested by centrifugation, resuspended in a buffer of 50 mM Tris-HCl, 250 mM NaCl, 5 mM imidazole, and 1 mM PMSF at pH 7.4, lysed by ultrasonication, and purified by Ni–NTA affinity chromatography. Following TEV proteolysis of the terminal His-tag, the samples were further purified on a Superdex75 size exclusion column. NMR samples were dialyzed into a buffer containing 20 mM NaPi, 80mM KCl, 1mM DTT, and 1mM EDTA at pH 7.4.

The full-length *Geo*Cas9 plasmid was acquired from Addgene (#87700), expressed in TB media and was expressed and purified as previously described.[2] The K267E, R332A, and K267E/R332A variants were introduced into full-length *Geo*Cas9 by modifying the original plasmid acquired from Addgene.

NMR spectroscopy

Backbone resonance assignments of *Geo*Rec1 and *Geo*Rec2 were carried out on a Bruker Avance NEO 600 MHz spectrometer at 25 °C. The following triple resonance experiments were collected for each sample: ^{1}H-^{15}N TROSY-HSQC, HNCA, HN(CO)CA, HN(CA)CB, HN(COCA)CB, HN(CA)CO and HNCO. All spectra were processed in NMRPipe[46] and analyzed in Sparky[47]. Three-dimensional correlations and assignments were made in CARA[48] and *Geo*Rec1 and *Geo*Rec2 backbone assignments were deposited in the BMRB under accession numbers 52363 and 51197, respectively. Backbone resonance assignments of *Geo*Rec were completed by transferring assignments from the individually assigned spectra of *Geo*Rec1 and *Geo*Rec2, as done previously for other large Cas9 fragments.[49,50]

NMR spin relaxation experiments were carried out in a temperature-compensated manner at 600 and 850 MHz on Bruker Avance NEO and Avance III HD spectrometers, respectively. CPMG experiments were adapted from the report of Palmer and coworkers[51] with a constant relaxation period of 20 ms and ν_{CPMG} values of 0, 25, 50, 75, 100, 150, 250, 500, 750, 800, 900, and 1000 Hz. Exchange parameters were obtained from global fits of the data carried out with RELAX[52] using the R2eff, NoRex, and CR72 models, as well as in-house fitting in GraphPad Prism with the following models:

Model 1: No exchange

$$R_2^{eff} = R_2^0 \quad (1)$$

Model 2: Two-state, fast exchange (Meiboom equation [53])

$$R_2^{eff} = R_2^0 + \frac{\Phi}{k_{ex}}\left[1 - \frac{4\nu_{CPMG}}{k_{ex}} \tan h\left(\frac{k_{ex}}{4\nu_{CPMG}}\right)\right] \quad (2)$$

Global fitting of CPMG profiles was determined to be superior to individual fits based on the Akaike Information Criterion.[54] Uncertainties in these rates were determined from replicate spectra with duplicate relaxation delays of 0, 25, 50 (×2), 75, 100, 150, 250, 500 (×2), 750, 800 (×2), 900, and 1000 Hz.

Longitudinal and transverse relaxation rates were measured with randomized T_1 delays of 0, 20, 60, 100, 200, 600, 800, and 1200 ms and T_2 delays of 0, 16.9, 33.9, 50.9, 67.8, 84.8, and 101.8 ms. Peak intensities were quantified in Sparky and the resulting decay profiles were analyzed in Sparky with errors determined from the fitted parameters. Uncertainties in these rates were determined from replicate spectra with duplicate relaxation delays of 20 (x2), 60 (x2), 100, 200, 600 (x2), 800, and 1200 ms for T_1 and 16.9, 33.9 (x2), 50.9 (x2), 67.8 (x2), 84.8, 101.8 (x2) ms for T_2. Steady-state ^{1}H-[^{15}N] NOE were measured with a 6 second relaxation delay followed by a 3 second saturation (delay) for the saturated (unsaturated) experiments and calculated by I_{sat}/I_{ref}. All relaxation experiments were carried out in a temperature-compensated interleaved manner.

Model-free analysis was carried out by fitting relaxation rates to five different forms of the spectral density function with local τ_m, spherical, prolate spheroid, oblate spheroid, or ellipsoid diffusion tensors.[55–60] The criteria for inclusion of resonances in the diffusion tensor estimate was based on the method of Bax and coworkers.[61] N-H bond lengths were assumed to be 1.02 Å and the ^{15}N chemical shift anisotropy tensor was −160 ppm. Diffusion tensor parameters were optimized simultaneously in RELAX under the full automated protocol.[52] Model selection was iterated until tensor and order parameters did not deviate from the prior iteration.

NMR titrations were performed on a Bruker Avance NEO 600 MHz spectrometer at 25 °C by collecting a series of ^{1}H-^{15}N TROSY HSQC spectra with increasing ligand (*i.e.* gRNA) concentration. The ^{1}H and ^{15}N carrier frequencies were set to the water resonance and 120 ppm, respectively. Samples of WT, K267E, and R332A *Geo*Rec were titrated with gRNA until no further spectral perturbations were detected. NMR chemical shift perturbations were calculated as:

$$\Delta\delta = \sqrt{(\Delta\delta_{HN}^2 + \Delta\delta_{NH}^2/25)/2}$$

Microscale thermophoresis (MST)

MST experiments were performed on a Monolith X instrument (NanoTemper Technologies), quantifying WT, K267E, R332A, and K267E/R332A *Geo*Rec binding to a 39-nt Cy5-labeled gRNA at a concentration of 20 nM in a buffer containing 20 mM sodium phosphate, 150 mM KCl, 5 mM $MgCl_2$, and 0.1% Triton X-100 at pH 7.6. The *Geo*Rec proteins were serially diluted from a 200 µM stock into 16 microcentrifuge tubes and combined in a 1:1 molar ratio with serially diluted gRNA from a 40 nM stock. After incubation for 5 minutes at 37 °C in the dark, each sample was loaded into a capillary for measurement. K_d values for the various complexes were calculated using the MO Control software (NanoTemper Technologies). Statistical significance was calculated using a two-tailed T-test.

Circular dichroism (CD) spectroscopy

All *Geo*Cas9 and *Geo*Rec proteins were buffer exchanged into a 20 mM sodium phosphate buffer at pH 7.5, diluted to 1 µM, and loaded into a 2 mm quartz cuvette (JASCO instruments). A CD spectrum was first measured between 200 - 250 nm, after which the sample was progressively heated from 20 – 90 °C in 1.0 °C increments while ellipticity was monitored at 222 and 208 nm.

Phosphate buffer baseline spectra were subtracted from the sample measurements. Prior to CD measurements, *Geo*Cas9-RNP was formed by incubating 3 µM *Geo*Cas9 with gRNA at a 1:1.5 molar ratio at 37 °C for 10 minutes. The unfolding CD data was fit in GraphPad Prism to:

$$Ellipticity\ (T) = \frac{[(m_f T + b_f) + (m_u T + b_u)] exp\left[\left(-\frac{\Delta H_{D,vH}}{R}\right)\left(\frac{1}{T} - \frac{1}{T_m}\right)\right]}{1 + exp\left[\left(-\frac{\Delta H_{D,vH}}{R}\right)\left(\frac{1}{T} - \frac{1}{T_m}\right)\right]}$$

X-ray crystallography

*Geo*Rec protein purified as described above was crystallized by sitting drop vapor diffusion at room temperature by mixing 1.0 µL of 15 mg/mL *Geo*Rec in a buffer of 20 mM HEPES and 100 mM KCl at pH 7.5 with 2.0 µL of crystallizing condition: 0.15 M calcium chloride, 15 % polyethylene glycol 6000, 0.1 M HEPES at pH 7.0. Crystals were cryoprotected in crystallizing condition supplemented with 30% ethylene glycol. Diffraction images were collected at the NSLS-II AMX beamline at Brookhaven National Laboratory under cryogenic conditions. Images were processed using XDS[62] and Aimless in CCP4.[63] Chain A of the *N. meningitidis* Cas9 X-ray structure (residues 249-445 only, PDB ID: 6JDQ) was used for molecular replacement with Phaser followed by AutoBuild in Phenix.[64] Electron density was only observed for the *Geo*Rec2 subdomain. The *Geo*Rec2 structure was finalized through manual building in Coot[65] and refinement in Phenix.

Molecular dynamics (MD) simulations

Molecular Dynamics (MD) simulations were based on the cryo-EM structure of full-length *Geo*Cas9 (PDB: 8UZA, resolution 3.17 Å) in complex with gRNA and target DNA with two mutations in *Geo*Cas9 (at residues 8 and 582). Four systems were considered for the MD studies: WT, K267E, R332A, K267E/R332A and i*Geo*Cas9. We generated the WT *Geo*Cas9 by back-mutating A8D and A582H from the cryo-EM structure (PDB: 8UZA), followed by introducing the mutations K267E, R332A, or a double mutation (with both K267E and R332A) for the variant systems. Subsequently, we performed MD simulation of i*Geo*Cas9 (PDB: 8UZB, resolution 2.63 Å) consisting of 10 mutations (D8A, E149G, T182I, N206D, P466Q, H582A, Q817R, E843K, E854G, K908R). All systems were solvated with explicit water in a periodic box of ~ 134 Å x ~ 154 Å x ~ 151 Å resulting in ~ 276,000 atoms. Counter ions were added to neutralize the systems. MD simulations were performed using a protocol tailored for protein-nucleic acid complexes,[66] previously applied in studies of CRISPR-Cas systems.[67–69] All the simulations were performed by using Amber ff19SB force field for protein,[70] ff99bsc1 corrections and χOL3 corrections for DNA and RNA, respectively.[71,72] Water molecules were described by TIP3P model.[73] All bonds involving hydrogens were constrained using the LINCS algorithm. A particle mesh Ewald method (PME) with a 10 Å cutoff was used to calculate electrostatics. Energy minimization was performed to relax the water molecules and counterions, keeping the protein-nucleic acid complex fixed with harmonic potential restraints of 100 kcal/mol $Å^2$. Equilibration was performed by gradually increasing the temperature from 0 to 100 K and then to 200 K in canonical NVT ensemble and isothermal-isobaric NPT ensemble. A final temperature of 300 K was maintained via Langevin dynamics with a collision frequency γ = 1/ps and a reference pressure of 1 atm was achieved through Berendsen barostat. Production runs were carried out in NVT ensemble for 2 µs for each system in three replicates, resulting in 6 µs per system (totaling 30 µs for all systems). The equations of motion were integrated with the leapfrog Verlet algorithm with a time step of 2 fs. All simulations were conducted using the GPU-empowered version of AMBER 22.[74] Analysis was performed on the aggregate ensemble (i.e., ~6 µs per system).

To characterize the protein-nucleic acid interactions in all the systems under investigation, we performed contact analysis. A contact was considered to form between two atoms within a cutoff distance of ≤4.5 Å. The binding free energy of gRNA and DNA with *Geo*Cas9 was calculated using the Molecular Mechanics Generalized Born Surface Area (MM-GBSA) method.[75–77] This

approach was used to compare the Rec-gRNA binding affinity of WT *Geo*Cas9 with its mutants. For each system, the binding energies were calculated over the ~200 ns ensemble of the stable trajectories at an interval of ~20 ns.

DNA cleavage assays

*Geo*Cas9 gRNA templates containing 21-nt spacers targeting the mouse *Tnnt2* gene locus were introduced into EcoRI and BamHI sites in pUC57 (Genscript). The plasmid was transformed into BL21(DE3) cells (New England BioLabs) and subsequent restriction digest of the plasmid DNA was carried out using the BamHI restriction enzyme (New England BioLabs) according to the manufacturer's instructions. Linearized plasmid DNA was immediately purified using the DNA Clean and Concentrator-5 kit (Zymo Research) according to the manufacturer's instructions. RNA transcription was performed *in vitro* with the HiScribe T7 High Yield RNA Synthesis Kit (New England BioLabs). DNA substrates containing the target cleavage site (479 base pairs, Figure S13) were produced by polymerase chain reaction (PCR) using mouse genomic DNA as a template and primer pairs 5'CAAAGAGCTCCTCGTCCAGT3' and 5' ATGGACTCCAGGACCCAAGA3' followed by a column purification using the NucleoSpin® Gel and PCR Clean-up Kit (Macherey-Nagel). For the *in vitro* activity assay, RNP formation was achieved by incubating 3 µM *Geo*Cas9 (WT, K267E, R332A, or K267E/R332A mutant) and 3 µM gRNA at either 37 °C, 60 °C, 75 °C, or 85 °C for 30 minutes in a reaction buffer of 20 mM Tris, 100 mM KCl, 5 mM $MgCl_2$, 1 mM DTT, and 5% glycerol at pH 7.5. The 10 µL cleavage reactions were set up by mixing RNP at varying concentrations with 149 nanograms of PCR products on ice followed by incubation at 37 °C for 30 minutes. The reaction was quenched with 1 µL of proteinase K (20 mg/mL) and subsequent incubation at 56 °C for 10 minutes. 6x DNA loading buffer was added to each reaction and 10 µL of reaction mixture per lane was loaded onto an agarose gel. DNA band intensity measurements were carried out with ImageJ.

For *in vitro* off-target activity assays, RNP formation was achieved by incubating 10 µM *Geo*Cas9 (WT, K267E, R332A, or K267E/R332A mutant) and 10 µM gRNA at 37 °C for 30 minutes in the reaction buffer described above. The 10 µL cleavage reactions were set up by mixing 1 µM RNP with 150 nanograms of PCR products (off-target DNA sequences listed in Table S2) on ice followed by incubation at 37 °C for varying time points. The reaction was quenched with 1 µL of proteinase K (20 mg/mL) and subsequent incubation at 56 °C for 10 minutes. 6x DNA loading buffer was added to each reaction and 10 µL of reaction mixture per lane was loaded onto an agarose gel. DNA band intensity measurements were carried out with ImageJ. WT and HiFi *Sp*Cas9 control proteins were purchased from Integrated DNA Technologies (IDT, cat. No. 108158 and No. 108160, respectively), as was the associated *Sp*Cas9 gRNA, Alt-R™ CRISPR-Cas9 gRNA, with an RNA spacer sequence complementing 5'-TGGACAGAGCCTTCTTCTTC-3'. The on-target and off-target DNA sequences used for the *Sp*Cas9 *in vitro* cleavage assay can be found in Table S3.

Acknowledgements

This work was supported by NIH grant R01 GM 136815 (to GP and GPL) and NSF grant MCB 2143760 (to GPL). GP acknowledges support from the NIH (Grant No. R01GM141329) and the NSF (CHE-2144823), as well as from the Sloan Foundation (FG-2023-20431) and the Camille and Henry Dreyfus Foundation (TC-24-063). This research used the AMX beamline of the National Synchrotron Light Source II, a U.S. Department of Energy (DOE) Office of Science User Facility operated for the DOE Office of Science by Brookhaven National Laboratory under Contract No. DE-SC0012704. The Center for BioMolecular Structure (CBMS) is primarily supported by NIGMS through a Center Core P30 Grant (P30 GM133893), and by the DOE Office of Biological and Environmental Research (KP1607011). Computational studies were carried out using Expanse at the San Diego Supercomputing Center through allocation MCB160059 and Bridges2 at the

Pittsburgh Supercomputer Center through allocation BIO230007 from the Advanced Cyberinfrastructure Coordination Ecosystem: Services & Support (ACCESS) program, which is supported by NSF grants #2138259, #2138286, #2138307, #2137603, and #2138296.

Additional information

Author Contributions

HBB and **ALK** produced *Geo*Rec2, *Geo*Rec1, *Geo*RecFL, and *Geo*Cas9 proteins and sgRNA, conducted the NMR and biophysical experiments, analyzed the data, and wrote the original draft of the manuscript. **AMD** solved the X-ray crystal structure of *Geo*Rec2. **CP** carried out MD simulations and analyzed the data. **ZF** and **JL** conducted *Geo*Cas9 functional assays and analyzed the data. **GP** supervised the MD studies and obtained funding. **GJ** supervised collection of X-ray crystallographic data. **GPL** conceived the study, supervised collection of NMR spectroscopic data, obtained funding, and wrote the original draft. The final manuscript was written and edited with contributions from all authors.

Additional files

Supporting Information

References

1 Belato H. B., et al. (2022) **Disruption of electrostatic contacts in the HNH nuclease from a thermophilic Cas9 rewires allosteric motions and enhances high-temperature DNA cleavage** *The Journal of Chemical Physics* **157** https://doi.org/10.1063/5.0128815

2 Harrington L. B., et al. (2017) **A thermostable Cas9 with increased lifetime in human plasma** *Nat Commun* **8**:1424 https://doi.org/10.1038/s41467-017-01408-4

3 Zhang S., et al. (2023) **Current Trends of Clinical Trials Involving CRISPR/Cas Systems** *Front. Med* **10** https://doi.org/10.3389/fmed.2023.1292452

4 Li T., et al. (2023) **CRISPR/Cas Therapeutics: Progress and Prospects** *Signal Trans. Targ. Ther* **8** https://doi.org/10.1038/s41392-41023-01309-41397

5 Kim E., et al. (2017) **In vivo genome editing with a small Cas9 orthologue derived from Campylobacter jejuni** *Nat Commun* **8** https://doi.org/10.1038/ncomms14500

6 Lee C. M., Cradick T. J., Bao G (2016) **The Neisseria meningitidis CRISPR-Cas9 System Enables Specific Genome Editing in Mammalian Cells** *Mol Ther* **24**:645–654 https://doi.org/10.1038/mt.2016.8

7 Belato H. B., et al. (2021) **Structural and dynamic insights into the HNH nuclease of divergent Cas9 species** *J Struct Biol* **214** https://doi.org/10.1016/j.jsb.2021.107814

8 Jinek M., et al. (2012) **A programmable dual-RNA-guided DNA endonuclease in adaptive bacterial immunity** *Science* **337**:816–821 https://doi.org/10.1126/science.1225829

9 Eggers A. R., et al. (2024) **Rapid DNA unwinding accelerates genome editing by engineered CRISPR-Cas9** *Cell* **187**:3249–3261 https://doi.org/10.1016/j.cell.2024.04.031

10 Palermo G., et al. (2018) **Key role of the REC lobe during CRISPR-Cas9 activation by 'sensing', 'regulating', and 'locking' the catalytic HNH domain** *Q Rev Biophys* **51** https://doi.org/10.1017/s0033583518000070

11 Dagdas Y. S., Chen J. S., Sternberg S. H., Doudna J. A., Yildiz A (2017) **A conformational checkpoint between DNA binding and cleavage by CRISPR-Cas9** *Sci Adv* **3**:eaao0027 https://doi.org/10.1126/sciadv.aao0027

12 Mir A., Edraki A., Lee J., Sontheimer E. J (2018) **Type II-C CRISPR-Cas9 Biology, Mechanism, and Application** *ACS Chem Biol* **13**:357–365 https://doi.org/10.1021/acschembio.7b00855

13 Jiang F., Zhou K., Ma L., Gressel S., Doudna J. A. STRUCTURAL BIOLOGY (2015) **A Cas9-guide RNA complex preorganized for target DNA recognition** *Science* **348**:1477–1481 https://doi.org/10.1126/science.aab1452

14 Sternberg S. H., LaFrance B., Kaplan M., Doudna J. A (2015) **Conformational control of DNA target cleavage by CRISPR-Cas9** *Nature* **527**:110–113 https://doi.org/10.1038/nature15544

15 Chen J. S., et al. (2017) **Enhanced proofreading governs CRISPR-Cas9 targeting accuracy** *Nature* **550**:407–410 https://doi.org/10.1038/nature24268

16 Skeens E., et al. (2024) **High-fidelity, hyper-accurate, and evolved mutants rewire atomic-level communication in CRISPR-Cas9** *Sci Adv* **10**:eadl1045 https://doi.org/10.1126/sciadv.adl1045

17 East K. W., et al. (2020) **Allosteric Motions of the CRISPR-Cas9 HNH Nuclease Probed by NMR and Molecular Dynamics** *Journal of the American Chemical Society* https://doi.org/10.1021/jacs.9b10521

18 Palermo G., Miao Y., Walker R. C., Jinek M., McCammon J. A (2016) **Striking Plasticity of CRISPR-Cas9 and Key Role of Non-target DNA, as Revealed by Molecular Simulations** *ACS Cent Sci* **2**:756–763 https://doi.org/10.1021/acscentsci.6b00218

19 Wu Z., Yang H., Colosi P (2010) **Effect of genome size on AAV vector packaging** *Mol Ther* **18**:80–86 https://doi.org/10.1038/mt.2009.255

20 Shen P., et al. (2024) **Structure of Geobacillus stearothermophilus Cas9: Insights into the Catalytic Process and Thermostability of CRISPR-Cas9** *ACS Catalysis* **14**:13227–13235

21 Eggers A. R., et al. (2024) **Rapid DNA Unwinding Accelerates Genome Editing by Engineered CRISPR-Cas9** *Cell* **187**:3249–3261

22 Lisi G. P., East K. W., Batista V. S., Loria J. P (2017) **Altering the allosteric pathway in IGPS suppresses millisecond motions and catalytic activity** *Proc Natl Acad Sci U S A* **114**:E3414–e3423 https://doi.org/10.1073/pnas.1700448114

23 Slaymaker I. M., et al. (2016) **Rationally engineered Cas9 nucleases with improved specificity** *Science* **351**:84–88 https://doi.org/10.1126/science.aad5227

24 Vakulskas C. A., et al. (2018) **A high-fidelity Cas9 mutant delivered as a ribonucleoprotein complex enables efficient gene editing in human hematopoietic stem and progenitor cells** *Nat Med* **24**:1216–1224 https://doi.org/10.1038/s41591-018-0137-0

25 Guzman I., Ghaemi Z., Baranger A., Luthey-Schulten Z., Gruebele M (2015) **Native Conformational Dynamics of the Spliceosomal U1A Protein** *The Journal of Physical Chemistry B* **119**:3651–3661 https://doi.org/10.1021/jp511760m

26 Doudna J. A., Charpentier E., Genome editing (2014) **The new frontier of genome engineering with CRISPR-Cas9** *Science* **346** https://doi.org/10.1126/science.1258096

27 Casini A., et al. (2018) **A highly specific SpCas9 variant is identified by in vivo screening in yeast** *Nat Biotechnol* **36**:265–271 https://doi.org/10.1038/nbt.4066

28 Ricci C. G., et al. (2019) **Deciphering Off-Target Effects in CRISPR-Cas9 through Accelerated Molecular Dynamics** *ACS Cent Sci* **5**:651–662 https://doi.org/10.1021/acscentsci.9b00020

29 Nierzwicki L., et al. (2021) **Enhanced specificity mutations perturb allosteric signaling in CRISPR-Cas9** *eLife* **10** https://doi.org/10.7554/eLife.73601

30 Nierzwicki Ł., et al. (2022) **Principles of target DNA cleavage and the role of Mg2+ in the catalysis of CRISPR–Cas9** *Nature Catalysis* **5**:912–922 https://doi.org/10.1038/s41929-022-00848-6

31 Shen P., et al. (2024) **Structure of Geobacillus stearothermophilus Cas9: Insights into the Catalytic Process and Thermostability of CRISPR-Cas9** *ACS Catalysis* **14**:13227–13235 https://doi.org/10.1021/acscatal.4c03278

32 Eggers A. R., et al. (2023) **Rapid DNA unwinding accelerates genome editing by engineered CRISPR-Cas9** *bioRxiv* :2023.2012.2014.571777 https://doi.org/10.1101/2023.12.14.571777

33 Doudna J. A (2020) **The promise and challenge of therapeutic genome editing** *Nature* **578**:229–236 https://doi.org/10.1038/s41586-020-1978-5

34 Palermo G., et al. (2017) **Protospacer Adjacent Motif-Induced Allostery Activates CRISPR-Cas9** *J Am Chem Soc* **139**:16028–16031 https://doi.org/10.1021/jacs.7b05313

35 Hou Z., et al. (2013) **Efficient genome engineering in human pluripotent stem cells using Cas9 from Neisseria meningitidis** *Proceedings of the National Academy of Sciences of the United States of America* **110**:15644–15649 https://doi.org/10.1073/pnas.1313587110

36 Kleinstiver B. P., et al. (2016) **High-fidelity CRISPR-Cas9 nucleases with no detectable genome-wide off-target effects** *Nature* **529**:490–495 https://doi.org/10.1038/nature16526

37 Hu J. H., et al. (2018) **Evolved Cas9 variants with broad PAM compatibility and high DNA specificity** *Nature* **556**:57–63 https://doi.org/10.1038/nature26155

38 Lee J. K., et al. (2018) **Directed evolution of CRISPR-Cas9 to increase its specificity** *Nat Commun* **9**:3048 https://doi.org/10.1038/s41467-018-05477-x

39 Ma E., Harrington L. B., O'Connell M. R., Zhou K., Doudna J. A (2015) **Single-Stranded DNA Cleavage by Divergent CRISPR-Cas9 Enzymes** *Mol Cell* **60**:398–407 https://doi.org/10.1016/j.molcel.2015.10.030

40 Nguyen V., et al. (2017) **Evolutionary drivers of thermoadaptation in enzyme catalysis** *Science* **355**:289–294 https://doi.org/10.1126/science.aah3717

41 Saavedra H. G., Wrabl J. O., Anderson J. A., Li J., Hilser V. J (2018) **Dynamic allostery can drive cold adaptation in enzymes** *Nature* **558**:324–328 https://doi.org/10.1038/s41586-018-0183-2

42 Shmakov S., et al. (2017) **Diversity and evolution of class 2 CRISPR-Cas systems** *Nat Rev Microbiol* **15**:169–182 https://doi.org/10.1038/nrmicro.2016.184

43 Venters R. A., Farmer B. T., Fierke C. A., Spicer L. D. (1996) **Characterizing the use of perdeuteration in NMR studies of large proteins: 13C, 15N and 1H assignments of human carbonic anhydrase II** *Journal of molecular biology* **264**:1101–1116 https://doi.org/10.1006/jmbi.1996.0699

44 Pervushin K., Riek R., Wider G., Wüthrich K (1997) **Attenuated T2 relaxation by mutual cancellation of dipole-dipole coupling and chemical shift anisotropy indicates an avenue to NMR structures of very large biological macromolecules in solution** *Proceedings of the National Academy of Sciences of the United States of America* **94**:12366–12371 https://doi.org/10.1073/pnas.94.23.12366

45 Tugarinov V., Kanelis V., Kay L. E (2006) **Isotope labeling strategies for the study of high-molecular-weight proteins by solution NMR spectroscopy** *Nat Protoc* **1**:749–754 https://doi.org/10.1038/nprot.2006.101

46 Delaglio F., et al. (1995) **NMRPipe: a multidimensional spectral processing system based on UNIX pipes** *J Biomol NMR* **6**:277–293 https://doi.org/10.1007/bf00197809

47 Lee W., Tonelli M., Markley J. L (2015) **NMRFAM-SPARKY: enhanced software for biomolecular NMR spectroscopy** *Bioinformatics* **31**:1325–1327 https://doi.org/10.1093/bioinformatics/btu830

48. Keller R. L. J. (2005) **Optimizing the process of nuclear magnetic resonance spectrum analysis and computer aided resonance assignment** *Doctoral Thesis thesis* ETH Zürich

49 Nerli S., De Paula V. S., McShan A. C., Sgourakis N. G (2021) **Backbone-independent NMR Resonance Assignments of Methyl Probes in Large Proteins** *Nat. Commun* **12**

50 De Paula V. S., Dubey A., Arthanari H., Sgourakis N. G (2024) **Dynamic Sampling of a Surveillance State Enables DNA Proofreading by Cas9** *Cell Chem. Biol* https://doi.org/10.1016/j.chembiol.2024.10.001

51 Loria J. P., Rance M., Palmer A. G (1999) **A Relaxation-Compensated Carr–Purcell–Meiboom–Gill Sequence for Characterizing Chemical Exchange by NMR Spectroscopy** *Journal of the American Chemical Society* **121**:2331–2332 https://doi.org/10.1021/ja983961a

52 Bieri M., d'Auvergne E. J., Gooley P. R. (2011) **relaxGUI: a new software for fast and simple NMR relaxation data analysis and calculation of ps-ns and µs motion of proteins** *J Biomol NMR* **50**:147–155 https://doi.org/10.1007/s10858-011-9509-1

53 Luz Z., Meiboom S (1963) **Nuclear Magnetic Resonance Study of the Protolysis of Trimethylammonium Ion in Aqueous Solution—Order of the Reaction with Respect to Solvent** *The Journal of Chemical Physics* **39**:366–370 https://doi.org/10.1063/1.1734254

54 Cavanaugh J. E., Neath A. A (2019) **The Akaike Information Criterion: Background, Derivation, Properties, Application, Interpretation, and Refinements** . *WIREs Comp. Mol. Sci* **11**:e1460

55 Brüschweiler R., Liao X., Wright P. E (1995) **Long-range Motional Restrictions in a Multidomain Zinc-finger Protein from Anisotropic Tumbling** *Science* **268**:886–889

56 Mandel A. M., Akke M., Palmer A. G (1995) **Backbone Dynamics of Escherichia coli Ribonuclease HI: Correlations with Structure and Function in an Active Enzyme** *J. Mol. Biol* **246**:144–163

57 Fushman D., Cahill S., Cowburn D (1997) **The Main-chain Dynamics of the Dynamin Pleckstrin Homology (PH) Domain in Solution: Analysis of 15N Relaxation with Monomer/Dimer Equilibration** *J. Mol. Biol* **266**:173–194

58 Orekhov V. Y., Korzhnev D. M., Diercks T., Kessler H., Arseniev A. S (1999) **1H-15N NMR Dynamic Study of an Isolated α-helical Peptide (1-36)bacteriorhodopsin Reveals the Equilibrium Helix-coil Transitions** *J. Biomol. NMR* **14**:345–356

59 Korzhnev D. M., Billeter M., Arseniev A. S., Orekhov V. Y (2001) **NMR Studies of Brownian Tumbling and Internal Motions in Proteins** *Prog. NMR Spectros* **38**:197–266

60 Zhuravleva A. V., et al. (2004) **Gated Electron Transfers and Electron Pathways in Azurin: A NMR Dynamic Study at Multiple Fields and Temperatures** *J. Mol. Biol* **342**:1599–1611

61 Tjandra N., Feller S. E., Pastor R. W., Bax A (1995) **Rotational Diffusion Anisotropy of Human Ubiquitin from N-15 NMR Relaxation** *J. Am. Chem. Soc* **117**:12562–12566

62 Kabsch W. (2010) **XDS** *Acta Crystallogr D Biol Crystallogr* **66**:125–132 https://doi.org/10.1107/s0907444909047337

63 Winn M. D., et al. (2011) **Overview of the CCP4 suite and current developments** *Acta Crystallogr D Biol Crystallogr* **67**:235–242 https://doi.org/10.1107/s0907444910045749

64 Liebschner D., et al. (2019) **Macromolecular structure determination using X-rays, neutrons and electrons: recent developments in Phenix** *Acta Crystallogr D Struct Biol* **75**:861–877 https://doi.org/10.1107/s2059798319011471

65 Emsley P., Lohkamp B., Scott W. G., Cowtan K. (2010) **Features and development of Coot** *Acta Crystallogr D Biol Crystallogr* **66**:486–501 https://doi.org/10.1107/s0907444910007493

66 Sinha S., Pindi C., Ahsan M., Arantes P. R., Palermo G (2023) **Machines on Genes through the Computational Microscope** *J. Chem. Theor. Comput* **19**:1945–1964

67 Saha A., et al. (2024) **An Alpha-helical Lid Guides the Target DNA Toward Catalysis in CRISPR-Cas12a** *Nat. Commun* **15** https://doi.org/10.1038/s41467-41024-45762-41466

68 Arantes P. R., et al. (2023) **Dimerization of the Deaminase Domain and Locking Interactions with Cas9 Boost Base Editing Efficiency in ABE8e** *Nucl. Acids Res* **52**:13931–13944

69 Sinha S., et al. (2024) **Unveiling the RNA-mediated Allosteric Activation Discloses Functional Hotspots in CRISPR-Cas13a** *Nucl. Acids Res* **52**:906–920

70 Tian C., et al. (2019) **f19SB: Amino-Acid-Specific Protein Backbone Parameters Trained against Quantum Mechanics Energy Surfaces in Solution** *J. Chem. Theor. Comput* **16**:528–552

71 Galindo-Murillo R., et al. (2016) **Assessing the Current State of Amber Force Field Modifications for DNA** *J. Chem. Theor. Comput* **12**

72 Zgarbova M., et al., Refinement of the Cornell, et al. (2011) **Nucleic Acids Force Field Based on Reference Quantum Chemical Calculations of Glycosidic Torsion Profiles** . *J. Chem. Theor. Comput* **7**:2886–2902

73 Jorgensen W. L., Chandrasekhar J., Madura J. D., Impey R. W., Klein M. L (1983) **Comparison of Simple Potential Functions for Simulating Liquid Water** *J. Chem. Phys* **79**:926–935

74 Case D. A., et al. (2005) **The Amber Biomolecular Simulation Programs** *J. Comput. Chem* **26**:1668–1688 https://doi.org/10.1002/jcc.20290

75 Mongan J., Simmerling C., McCammon J. A., Case D. A., Onufriev A (2007) **Generalized Born Model with a Simple, Robust Molecular Volume Correction** . *J. Chem. Theor. Comput* **3**:156–169

76 Nguyen H., Pérez A., Bermeo S., Simmerling C (2015) **Refinement of Generalized Born Implicit Solvation Parameters for Nucleic Acids and their Complexes with Proteins** *J. Chem. Theor. Comput* **11**:3714–3728

77 Nguyen H., Roe D. R., Simmerling C (2013) **Improved Generalized Born Solvent Model Parameters for Protein Simulations** *J. Chem. Theor. Comput* **9**:2020–2034

Author information

Helen B Belato[#]
Department of Molecular Biology, Cell Biology & Biochemistry, Brown University, Providence, United States

[#]These authors contributed equally to this work

Alexa L Knight[#]
Department of Molecular Biology, Cell Biology & Biochemistry, Brown University, Providence, United States

[#]These authors contributed equally to this work

Alexandra M D'Ordine
Department of Molecular Biology, Cell Biology & Biochemistry, Brown University, Providence, United States

Chinmai Pindi
Departments of Bioengineering and Chemistry, University of California Riverside, Riverside, United States

Zhiqiang Fan
Departments of Bioengineering and Chemistry, University of California Riverside, Riverside, United States

Jinping Luo
Departments of Bioengineering and Chemistry, University of California Riverside, Riverside, United States

Giulia Palermo
Departments of Bioengineering and Chemistry, University of California Riverside, Riverside, United States

Gerwald Jogl
Department of Molecular Biology, Cell Biology & Biochemistry, Brown University, Providence, United States

George P Lisi
Department of Molecular Biology, Cell Biology & Biochemistry, Brown University, Providence, United States, Brown University RNA Center, Providence, United States
ORCID iD: 0000-0001-8878-5655

For correspondence: george_lisi@brown.edu

Editors

Reviewing Editor
Julien Roche
Iowa State University, Ames, United States of America

Senior Editor
Amy Andreotti
Iowa State University, Ames, United States of America

Reviewer #1 (Public review):

Summary:

In this study from Belato, Knight and co-workers, the authors investigated the Rec domain of a thermophilic Cas9 from Geobacillus stearothermophilus (GeoCas9). The authors investigated three constructs, two individual subdomains of Rec (Rec1 and Rec2) and the full Rec domain. This domain is involved in binding to the guide RNA of Cas9, as well as the RNA-DNA duplex that is formed upon target binding. The authors performed RNA binding and relaxation experiments using NMR for the wild-type domain as well as two-point mutants. They observed differences in RNA binding activities as well as the flexibility of the domain. The authors also performed molecular dynamics and functional experiments on full-length GeoCas9 to determine whether these biophysical differences affect the RNA binding or cleavage activity. Although the authors observed some changes in the thermal stability of the mutant GeoCas9-gRNA complex, they did not observe substantial differences in the guide RNA binding or cleavage activities of the mutant GeoCas9 variants.

Overall, this manuscript provides a detailed biophysical analysis of the GeoCas9 Rec domain. The NMR assignments for this construct should prove very useful, and can serve as the basis for future similar studies of GeoCas9 Rec domain mutants. While the two mutants tested in the study did not produce significant differences from wild-type GeoCas9, the study rules out the possibility that analogous mutations can be translated between type II-A and II-C Cas9 orthologs. Together, these findings may provide the grounds for future engineering of higher fidelity variants of GeoCas9

https://doi.org/10.7554/eLife.99275.2.sa3

Reviewer #2 (Public review):

The manuscript from Belato et al., used advanced NMR approaches and a mutagenesis campaign probe the conformational dynamics of the recognition lobe (Rec) of the CRISPR Cas9 enzyme from G. stearothermophilus (GeoCas9). Using truncated and full-length constructs they assess the impacts of two different point mutations have on the redistribution and timescale of these motions and assess gRNA recognition and specificity. Single point mutations in the Rec domain in a Cas9 from a related species had profound impacts on- and off-target DNA editing, therefore the authors reasoned analogous mutations in GeoCas9

would have similar effects. However, despite a redistribution of local motions and changes in global stability, their chosen mutations had little impact on DNA editing in the context of the full-length enzyme.

In their revised manuscript, the authors were highly responsive to the reviewer's comments incorporating new experimental results including molecular dynamics simulations and RNA binding data using full-length GeoCas9, as well as reframing their discussion and conclusions in consideration of the new data. They were receptive to suggestions for clarification in both the text and methods section. With these changes, the manuscript has been significantly improved.

Their studies highlight the species-specific complexity of interdomain communication and allosteric mechanisms used by these multi-domain endonucleases. The noted strengths of the article remain, and despite the negative results, their approach will garner interest from investigators interested in understanding how the activity and specificity of these enzymes can be engineered to tune activity and limit off-target cleavage by these enzymes. Generally, the manuscript highlights the challenges of studying the effect of allosteric networks on protein function, particularly in multidomain proteins, and thus will be of broad interest to the community.

https://doi.org/10.7554/eLife.99275.2.sa2

Reviewer #3 (Public review):

The authors explore the role of Rec domains in a thermophilic Cas9 enzyme. They report on the crystal structure of part of the recognition lobe, its dynamics from NMR spin relaxation and relaxation-dispersion data, its interaction mode with guide RNA, and the effect of two single-point mutations hypothesised to enhance specificity. They find that mutations have small effects on Rec domain structure and stability but lead to significant rearrangement of micro- to milli-second dynamics which does not translate into major changes in guide RNA affinity or DNA cleavage specificity, illustrating the inherent tolerance of GeoCas9. The work can be considered as a first step towards understanding motions in GeoCas9 recognition lobe, although no clear hotspots were discovered with potential for future rational design of enhanced Cas9 variants.

Strengths:

- Detailed biophysical and structural investigation, despite a few technical limitations inherent with working with complex targets, provides converging evidence that molecular dynamics embedded in the recognition lobes allow GeoCas9 to operate on a broad range of substrates.
- Since the authors and others have shown that substrate specificity is dictated by equivalent hotspot mutations in other Cas9 variants, we are one step closer to understanding this phenomenon.

Weaknesses:

- Since the mutations investigated here do not significantly affect substrate binding or enzymatic activity, it is difficult to rationalize anything for enzyme engineering at this point.
- Further investigation of the determinants of the observed dynamic modes, and follow-up with rationally designed mutations would hopefully allow to create a real model of the mechanism, but I do understand that this goes beyond the scope of this study.

https://doi.org/10.7554/eLife.99275.2.sa1

Author response:

The following is the authors' response to the original reviews

> ***Public Reviews:***
>
> ***Reviewer #1 (Public Review):***
>
> *Summary:*
>
> *In this study from Belato, Knight, and co-workers, the authors investigated the Rec domain of a thermophilic Cas9 from Geobacillus stearothermophilus (GeoCas9). The authors investigated three constructs, two individual subdomains of Rec (Rec1 and Rec2) and the full Rec domain. This domain is involved in binding to the guide RNA of Cas9, as well as the RNA-DNA duplex that is formed upon target binding. The authors performed RNA binding and relaxation experiments using NMR for the wild-type domain as well as two-point mutants. They observed differences in RNA binding activities as well as the flexibility of the domain. The authors also performed experiments on fulllength GeoCas9 to determine whether these biophysical differences affect the RNA binding or cleavage activity. Although the authors observed some changes in the thermal stability of the mutant GeoCas9-gRNA complex, they did not observe substantial differences in the cleavage activities of the mutant GeoCas9 variants.*
>
> *Overall, this manuscript provides a detailed biophysical analysis of the GeoCas9 Rec domain. The NMR assignments for this construct should prove very useful, and the results may provide the grounds for future engineering of higher fidelity variants of GeoCas9. While the NMR results are generally well presented, it is unclear how the results on the isolated Rec domain related to the overall function of full-length GeoCas9. In addition, some conclusions are overstated and not fully supported by the evidence provided. The following major points should be addressed by the authors.*
>
> *(1) Many of the results rely on the backbone resonance assignments of the three constructs that were used, and the authors have done an excellent job of assigning the Rec1 and Rec2 constructs. However, it is unclear from the descriptions in the text how the full-length Rec construct was assigned. Were these assignments made based on assignments for the individual domains? The authors state that the spectra of individual domains and RecFL overlay very well, but there appear to be many resonances that have chemical shift differences or are only present in one construct. As it stands, it is unclear how the resonances were assigned for residues whose chemical shifts were perturbed, making it difficult to interpret many of the results.*

The Reviewer raises an important oversight. In Lines 491-493, we clarify that we were able to transfer the assignments using spectral overlays of the individual domains with *Geo*Rec (i.e. careful analysis of the data in Figure S3). We also cite two new references where a similar approach was applied to Cas9.

> *(2) The minimal gRNA that was used for the Rec-gRNA binding experiments is unlikely to be a good mimic for the full-length gRNA, as it lacks any of the secondary structure that is most specifically recognized by the REC lobe and the rest of the Cas9 protein. The majority of this RNA is a "spacer" sequence, but spacers are variable, so this sequence is arbitrary. Thus, the interactions that the authors are observing most likely represent non-specific interactions between the Rec domains and RNA. The authors also map chemical shift perturbations and line broadening on structural models with an RNA-DNA duplex bound, but this is not an accurate model for how the Rec domain binds to a single-stranded RNA (for which there is no structural model). Thus, many of the conclusions regarding the RNA binding interface are overstated.*

The Reviewer again raises an important point. We have added a section of text explaining the rationale for truncating the gRNA for binding experiments with NMR (Lines 223-235). We chose the 5'end of the gRNA containing the spacer sequence based on crystal structures of *Nme*Cas9 and *Sp*Cas9 that show the Rec lobe interacting with this section of nucleic acid. The newly published *Geo*Cas9 cryo-EM structure bound to gRNA, which overlaid well with the *Nme*Cas9 structure, also suggested that this portion of the gRNA could interact with Rec.

Figures S11 and S12 show our gradual truncation of the gRNA and Rec construct to achieve useful atomic detail. Ultimately, a 39nt gRNA containing a 23 base pair spacer sequence was chosen for this study to retain the NMR signal of the complex and because several structures suggested this 39nt sequence would be long enough to interact with the entire Rec lobe.

To investigate the effect of the spacer sequence, we have now measured binding affinities via MST between *Geo*Rec and a 39nt Tnnt2 gRNA and a 39nt gRNA from PDB: 8UZA, containing a different spacer sequence used in the very recent *Geo*Cas9 cryo-EM structure. The observed trends for each gRNA are consistent across the samples. We also measured WT, K267E, and R332A *Geo*Cas9 affinity for the full-length Tnnt2 and PDB:8UZA gRNAs.

Lastly, we used a new cryo-EM structure of *Geo*Cas9 bound to gRNA (PDB: 8JTR) to better define the interface for NMR CSPs and line broadening and have adjusted the language in this section.

> *(3) The authors include microscale thermophoresis (MST) data for the Rec constructs binding to the minimal gRNA. These data suggest that all three Rec variants have very similar Kd's for the RNA. Given these similarities, it is unclear why the RNA titration experiments by NMR yielded such different results. Moreover, in the Discussion, the authors state that the NMR titration data are consistent with the MST-derived Kd values. This conclusion appears to be overstated given the very small differences in affinities measured by MST.*

MST and NMR experiments describing the weakened binding affinity of *Geo*Rec and *Geo*Rec2 for the Tnnt2 gRNA agree with each other (Figure 5). However, additional MST experiments with a different gRNA sequence (from PDB: 8UZA) and with fulllength *Geo*Cas9 (new Figure 7) have provided new insight for us to soften and reframe the Discussion to avoid overstatement. See Lines 263-282 and 375-385.

> *(4) While the authors have performed some experiments to help place their findings on the isolated Rec domain in the context of the full-length protein, these experiments do not fully support the conclusions that the authors draw about the meaning of their NMR results. The two Cas9 variants that were explored via NMR have no effect on Cas9 cleavage activity, and it is unclear from the data provided whether they have any effect on GeoCas9 binding to the full sgRNA. This makes it difficult to determine whether the observed differences in RNA binding and dynamics of the isolated Rec domain have any consequence in the context of the full protein.*

We have since measured the binding affinities of full-length *Geo*Cas9 to full-length gRNA. (new Figure 7) We have also added a comment in the Discussion section describing how both *Geo*Rec and *Geo*Rec2 domain variants bind the truncated RNA with weaker affinity than the WT, but this biophysical effect does not translate to *Geo*Cas9 with its full-length gRNA. We describe this finding as an explanation for why the single-point mutants have minimal effect of *Geo*Cas9 cleavage activity. See Lines 375-385.

> *(5) The authors state in multiple places that the K267E/R332A mutant enhanced GeoCas9 specificity. Improved specificity refers to a situation in which the efficiency of cleavage of*

a perfectly matched target improves in comparison to a mismatched target. This is not what the authors observed for the double mutant. Instead, the cleavage of the perfect target was drastically reduced, in some cases to a larger degree than for the mismatched target. The double mutant does not appear to have improved specificity, it has simply decreased cleavage efficiency of the enzyme.

The conclusion has been reframed to suggest that the K267E/R332A double mutant has decreased cleavage efficiency of the enzyme but does not enhance *Geo*Cas9 specificity. We discuss an interesting contrast, namely that mutations in the *Sp*Cas9 Rec lobe alter its specificity, which is at times accompanied by a loss of overall activity. We also speculate on why this may not be the case in *Geo*Cas9, considering some very recent (unpublished at the time of initial submission) structural and biochemical data. See Lines 414-418.

Reviewer #2 (Public Review):

Summary:

The manuscript from Belato et al. used advanced NMR approaches and a mutagenesis campaign to probe the conformational dynamics of the recognition lobe (Rec) of the CRISPR Cas9 enzyme from G. stearothermophilus (GeoCas9). Using truncated and full-length constructs they assess the impacts of two different point mutations have on the redistribution and timescale of these motions and assess gRNA recognition and specificity. Single point mutations in the Rec domain in a Cas9 from a related species had profound impacts on- and off-target DNA editing, therefore the authors reasoned analogous mutations in GeoCas9 would have similar effects. However, despite a redistribution of local motions and changes in global stability, their chosen mutations had little impact on DNA editing in the context of the full-length enzyme. Their studies highlight the species-specific complexity of interdomain communication and allosteric mechanisms used by these multi-domain endonucleases. Despite these negative results, their study is highly rigorous, and their approach will broadly support understanding how the activity and specificity of these enzymes can be engineered to tune activity and limit off-target cleavage by these enzymes.

Strengths:

(1) Atomistic investigation of the conformational dynamics of the GeoCas9 gRNA recognition lobe (GeoRec), probing dynamics on a broad range of timescales from ps to ms using advanced NMR approaches will be broadly interesting to both the structural biology and CRISPR engineering communities.

(2) Highly rigorous biophysical studies that push the boundaries of current techniques, provide insight into local dynamics of the GeoRec domain that serve to propagate allosteric information and potentially regulate enzymatic activity.

(3) The study highlights the complexities of understanding interdomain communication in Cas9 enzymes since analogous mutations in different species have different effects on target recognition and cleavage.

(4) The type of structural and dynamic insights derived from this study design could serve as foundational information to guide a rational design strategy aimed at improving the selectivity and reducing the off-target effects of Cas9 enzymes.

Weaknesses:

(1) Despite the rigor of the experiments, the mutations chosen by the authors do not have a profound effect on the overall substrate affinity or activity of GeoCas9 rendering little mechanistic insight into allosteric communication in this particular Cas9. However, the

> *double mutant K267E/R332A has a more pronounced effect on the cleavage of WT and mismatched (at nucleotides 19 and 20) DNA substrates while minimally affecting the cleavage of mismatched (at nucleotides 5 and 6), suggesting more could be learned about the allosteric mechanism from the detailed characterization of this mutant.*

We thank the Reviewer for this comment. While we have included new binding experiments with full-length *Geo*Cas9 and gRNAs (new Figure 7), the addition of new MD simulations (new Figure 6) better address this point. MD examined our single and double mutants, as well as the recently published high-specificity i*Geo*Cas9, and reported the degree of conformational sampling and nucleic acid contacts and binding energies.

The simulations show that our mutations induce some, but not the full extent of the effect of i*Geo*Cas9 (with one mutation in *Geo*Rec and many others in the adjacent WED domain), implying that further engineering of *Geo*Rec to mimic i*Geo*Cas9's properties can have profound functional outcomes. Future efforts to mutate *Geo*Rec will be leverage this strategy. See Lines 309-342.

> *(2) Follow-up experiments with other residues that were identified as being highly dynamic might affect substrate recognition and cleavage activity in different ways providing additional insight.*

The Reviewer is correct. While beyond this initial scope, new MD simulations (see the response directly above) and NMR resonances distally affect by gRNA (via CSP or relaxation dispersion) will be used identify the primary targets for this analysis.

> *(3) Details regarding the authors' experimental approach are incomplete such as a description of the model used to fit the CD data, a detailed explanation of the global fitting of the relaxation dispersion data describing how the best-fit model was selected, and the description of the ModelFree fitting of fast timescale dynamics is incomplete.*

We thank the Reviewer for pointing out these oversights. We have now included the fitting equation in the CD Methods section.

We included new Figures S8-S10 with the individual relaxation dispersion curves and note in the Methods that global fits were deemed superior based on the Akaike Information Criterion. For WT, the AIC showed the global fit to be ~10-fold better. For K267E, the global model was 4-fold better, and for R332A, the global model was 6-fold better.

We have included a more detailed description of CPMG and Model-free fitting. See Lines 520-526.

> ***Reviewer #3 (Public Review):***
>
> *The authors explore the role of Rec domains in a thermophilic Cas9 enzyme. They report on the crystal structure of part of the recognition lobe, its dynamics from NMR spin relaxation and relaxation-dispersion data, its interaction mode with guide RNA, and the effect of two single-point mutations hypothesised to enhance specificity. They find that mutations have small effects on Rec domain structure and stability but lead to significant rearrangement of micro- to milli-second dynamics which does not translate into major changes in guide RNA affinity or DNA cleavage specificity, illustrating the inherent tolerance of GeoCas9. The work can be considered as a first step towards understanding motions in GeoCas9 recognition lobe, although no clear hotspots were discovered with potential for future rational design of enhanced Cas9 variants.*

> ***Recommendations for the authors:***
>
> ***Reviewer #1 (Recommendations For The Authors):***
>
> *Suggestions for improved or additional experiments, data, or analyses*

(1) Please update the sentences on lines 100-105 and the Methods to clarify how the RecFL assignments were obtained. If RecFL was assigned based on the assignments for Rec1 and Rec2, please describe in the Methods how the shifted resonances were handled. Please also provide chemical shift perturbation profiles for the truncated constructs versus the full-length Rec construct.

We have now added text (Lines 491-493) and two new references explaining the *Geo*Rec (full-length) assignment.

We appreciate this point. We have now provided a new Figure S9 with analysis of CSPs and line broadening in truncated constructs (*Geo*Rec2 only). See also Lines 263-282. We also show a similar structural response to mutation in full-length *Geo*Rec and *Geo*Rec2 NMR CSPs (Figure 2 and Figure S5).

We have provided the CSPs for each construct, relative to the full-length *Geo*Rec domain, Author response image 1. In most cases, the largest CSPs occur at resonances on the periphery of the spectra, retaining the ability to unambiguously assign it.

Author response image 1.

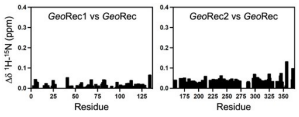

> *(2) It is unclear whether the differences in Kd's for the Rec-gRNA interactions are statistically significant, given the errors associated with the values. Can the authors further analyze these data to determine statistical significance? If they are not found to be significantly different, the authors should soften all conclusions related to the observed differences.*

Statistical significance was calculated for all MST data and Figures 5 and 7 have been updated to reflect this

> *(3) As mentioned above, it seems likely that the Rec-RNA binding that is observed is non-specific. Have the authors tried MST with another 39 nt RNA? Are there differences in affinities for the Rec constructs?*

We have done MST with another 39nt RNA. The affinity for each gRNA (Tnnt2 vs 8UZA) is similar for WT and K267E, and a factor of ~4 weaker for R332A with 8UZA gRNA. The trend is the same, that WT Rec has a (statistically significant) stronger affinity for the gRNA compared to the mutants.

> *(4) Have the authors tried MST with full-length GeoCas9 and the sgRNA? The current data on the thermal stability of the RNP's is interesting, but a more direct measurement of the affinity of the Cas9-sgRNA complexes would provide stronger evidence of the effects of the mutations.*

The Reviewer makes an excellent suggestion. We have now generated Cy5-labeled full-length gRNAs and conducted MST with full-length *Geo*Cas9 (new Figure 7). The binding affinities to multiple guides do not vary significantly. We have discussed this, and its implications, in Lines 376-385.

> *(5) One potential issue with not observing differences between the three Cas9 variants' cleavage activity is that the activity of these purified proteins appears to be very low in comparison to previous studies of GeoCas9. There are significant differences in the expression protocol used by the authors of the current study and previous studies. Have the authors attempted to replicate the expression and purification protocol of previous reports? This may improve the enzymatic activity and allow for a more detailed investigation of cleavage between the three variants (e.g. by performing time-course cleavage assays).*

The expression protocol of *Geo*Cas9 is identical to those of previous studies. This was a written mistake on our part, which has now been corrected in the methods section. We apologize for this oversight.

> *Recommendations for improving the writing and presentation*
>
> *The introduction of the manuscript is reasonable for specialists who are very familiar with Cas9 function, but it does not contain important details that may be unknown to most readers. The authors do not introduce the domains of Cas9 in the Introduction section. A brief description of the domains that are important to this work should be provided. For example, what is the role of the Rec lobe? This is not introduced until lines 110-111, after some discussion of the authors' initial work on these domains. For a broad audience, it would also be helpful to define the two catalytic domains of the protein. A paragraph describing the general architecture of Cas9 and the overall mechanism of Cas9, including allostery and domain movement, would be very helpful to a general audience. There are elements of this throughout the manuscript, but it would be better to have everything described in a single location at the beginning of the Introduction.*

The Reviewer makes an excellent point. We have added significant clarifying text to the Introduction (Lines 42-47, 52-58, and 61-66). We have also amended Figure 1 to highlight the domain arrangement of *Geo*Cas9 and construct domain boundaries.

Minor corrections to the text

> *(1) Lines 37-38: The statement about GeoCas9 activity should reference citation.*

We have added two references here.

> *(2) Line 39-40: "The widely-studied SpCas9, as well as GeoCas9, are Type-II CRISPR systems". Cas9 is only a single component of a larger system that contains other proteins and DNA elements, so it would be more appropriate to say "are effectors of type II CRISPR systems" or "are signature proteins of type II CRISPR systems". Also, please define the organism from which SpCas9 is derived. It may be more appropriate to use the three-letter abbreviation "SpyCas9" to be consistent with the abbreviation used for GeoCas9.*

We have revised the initial suggestion and specified the organisms. We have, however, chosen to keep "*Sp*Cas9" for consistency with our prior work and the work of many several others, including Doudna et al and Zhang et al.

> *(3) Lines 39-42: "only the Type II-C class to which GeoCas9 belongs has been rigorously validated for mammalian genome editing". SpCas9 is from a type II-A system and is by far the most commonly used ortholog for genome editing, including in ongoing clinical trials. It is unlikely that any of the type II-C Cas9 orthologs have been more rigorously validated than SpCas9. The reference cited in this sentence also does not support this statement and is a review written in 2017, so would be unlikely to reflect the current state of the art. Please revise this sentence.*

We have softened and revised this text (Lines 42-47).

> *(4) Lines 48-52: It would be helpful to describe the dynamic movement of the HNH domain (and cite appropriate references) prior to describing the authors' previous work. As it stands, it is unclear how this sentence would be understood by a non-specialist.*

We have added text in Lines 61-68

> *(5) Lines 44-45: The wording is a little unclear, as it sounds like the guide RNA, rather than the nuclease domains, is responsible for dsDNA cleavage. The sentence could be adjusted to remove "and cleave". Cleavage by the HNH and RuvC domains could be described in a separate sentence.*

We have revised this text. See Lines 49-50.

> *(6) Lines 46-48: This segment of the sentence suggests that PAM recognition triggers the allosteric events that result in the movement of the nuclease domain (HNH). This is misleading, as HNH movement is triggered by the complete formation of an R-loop, rather than initial PAM recognition. Please revise this sentence.*

We have revised the text in Lines 52-58.

> *(7) Lines 62-65: The first sentence is unclear. The specificity of many protein-nucleic acid complexes is well understood and is also readily quantified by several wellestablished methods. Are the authors specifically referring to the structural basis for Cas9 specificity? Although Cas9 specificity is highly complex, it has been studied structurally in great detail and should not be described as "poorly understood" without some discussion of what is already known. These sentences also elide the fact that Cas9 specificity has been successfully altered via rational design, based on our general framework for understanding protein-nucleic acid interactions. Please clarify these statements.*

The Reviewer makes an important point. We have softened this statement (Lines 8081). We have clarified that we intended to refer to structural characterization of large, multidomain proteins and nucleic acid complexes via NMR. We agree that many critical structural studies comment on Cas9 dynamics and specificity in great detail, including at the domain-level.

> *(8) Lines 62-68: It seems like the citations do not match up with the references in this section. The references for citations 8-10 are not about DNA repair complexes, references 11-14 are not papers about the directed evolution of Cas9 (should these be 16-17?), and the references for the HNH domain movements should be for citations 1821.*

We apologize for the confusion, and the references have been updated

> *(9) Lines 116-119: The description of the RNAs used is unclear, as the segments that are described add up to 141 not 101. Also, what is meant by "110-nt guide sequence intrinsic*

> *to GeoCas9"? Is this referring to the tracrRNA segment? It may be helpful if the RNA sequences shown in the accompanying figures were replaced with cartoons of the RNAs that were used, with the different segments labeled.*

We now describe the gRNA sequences in detail in new Table S4. We also expanded a bit in the text (Lines 224-235).

> *(10) Line 121-123: This sentence should contain reference(s).*

We have changed the sentence.

> *(11) Line 156-158: Reference 19 did not report or investigate any higher specificity SpCas9 variants, is this citation correct?*

We have removed the reference from this line. Ref. 19 (now Ref 23, Slaymaker *et al*) should be correct.

> *(12) Lines 162-166: Please provide a sequence and structural alignment for SpCas9 and GeoCas9 to support the claim that the amino acid substitutions are equivalent between the two orthologs.*

We have updated Figure 1 to display the similarity in domain arrangement between *Sp*Cas9 and *Geo*Cas9 and have noted similarity in structure and sequence of these proteins in Figure S1.

> *(13) Lines 234-236: There is insufficient evidence to conclude that the alterations in protein dynamics caused the changes in gRNA interaction. The substitutions are charge swap substitutions, and it is equally (if not more) feasible that these substitutions decrease the potential for favorable electrostatic interactions.*
>
> *(14) Lines 261-265: While the RNP stability for R332A is clearly decreased in comparison to WT, the authors' conclusions regarding K267E seem overstated. The difference in Tm for the K267E mutant and WT RNPs is not very large and may be within error, especially given that the CD data are noisy. Similarly, on lines 321-322, only one of the mutations really impacted the stability of the full-length RNP.*

We have softened this text in Lines 303-305.

> *(15) Lines 336-338: HiFi-SpCas9 does not contain four mutations, it is a single R691A point mutation, as reported in reference 17. This sentence and subsequent sentences should be updated.*

Here, the “final form” of HiFi *Sp*Cas9 contains the R691A and three additional mutations. The Reviewer is correct, though, that the R691A mutation alone was enough to enhance the specificity of WT *Sp*Cas9. We have clarified this point on Line 156.

> *Minor corrections to the figures*
>
> *(16) The cryo-EM structures of GeoCas9 have recently been released on the PDB. The authors may now update figures to include the experimentally determined structure, rather than an AlphaFold model and update the text accordingly.*

We have made this change.

> *(17) For Figure S4, please describe what the red dashed lines are in the top three graphs. Are these the Tm values determined for the two individual Rec domains? How do these compare to the inflection points for the two transitions in the full Rec construct (could be determined by plotting the first derivative data)? Please provide information in the Methods on how the temperature-dependent CD spectral data were fit and Tm's were determined.*

We have made these changes in the Figure S4 caption and Methods section.

> *(18) The blue box denoting the unassigned region is missing from Figure 2C-D, although it is mentioned in the figure legend.*

We have added the blue box denoting the unassigned linker.

> ***Reviewer #2 (Recommendations For The Authors):***
>
> *The manuscript is well-written and generally clear and concise. The following recommendations will help improve the readability and include details important for interpreting the results.*
>
> *(1) In general, the figures are too small and difficult to interpret, it was hard to discern the differences described in the text (e.g. Figure 1A, E, 4A, etc.), the text labels are illegible in several panels (e.g. Figure 4A, S8B, C, etc.), the chosen colors were difficult to interpret in the structures (Figure 4C, S8G, H, etc.), as well as residues with motion (as balls) were difficult to make out due to size and color usage. Similar story for the dispersion curves (Fig 3A), the plots are chaotically crowded, and it is impossible to interpret (or see) the undelaying data.*

We apologize for these difficulties. We have now revised the Figures in several ways. First, we greatly simplified Figure 1, such that it now includes only the domain arrangement, structure, and initial NMR details for *Geo*Rec (essentially A-B of the old Figure 1).

Second, we have reformatted Figure 3 to make the structure maps a bit easier to see.

We certainly appreciate the point made by the Reviewer about the dispersion curves. Our intent here is to illustrate the number of curves that can be fit globally, which substantially increase for K267E and R332A *Geo*Rec3, versus WT. As a compromise, we have included the individual dispersion curves in the SI for each variant. We have also thinned the line weights for each fit, and added NMR order parameters to the main figure to round out the discussion of dynamics.

Third, we have compiled the gRNA titration into Figure 4, removing the CD analysis (to SI), MST data (new Fig 5), and unclear structure maps to focus only on the NMR spectra here.

Fourth, we have created a new Figure 5 focusing on MST studies of two gRNAs with *Geo*Rec, which now include bar charts of affinities with appropriate statistics.

Much of the data trimmed from the prior version of the manuscript figures has been moved to Supporting Information. We have also created two new main text Figures (6 & 7) based on MD simulations and MST studies of full-length *Geo*Cas9 and gRNAs to provide additional context for interpreting the results in prior figures.

> *(2) Line 39 - this sentence is awkward, could you rephrase it?*

We have rephrased this sentence.

> *(3) There is inconsistent labeling, in Figure S2 the full-length construct is referred to as GeoRecFL while in other places in the text and in Figure 1 it is called GeoRec.*

We have changed all references to the intact Rec lobe to "*Geo*Rec."

> *(4) It would be helpful to include a cartoon of the domain organization of GeoCas9 and indicate the truncation mutants that were studied in this manuscript.*

We included the domain organization in Figure 1A and indicated the amino acid boundaries for each construct on the figure and in the Methods section.

> *(5) There is significant line broadening that occurs during the titration, not all line broadening is due to changes in rotational correlation time, and differential line broadening may reveal interactions of residues that are in the intermediate regime, certainly, uM affinities measured by the authors, would suggest this, therefore, a plot of I/Io might inform on binding sites, and it might be useful to look at differential broadening as a function of titrant added.*

The Reviewer makes a very good point. In addition to the data in Figure 4, which show a clear reduction in gRNA-induced line broadening in larger *Geo*Rec constructs, we included new titration data on smaller *Geo*Rec2 domains (Figure S12). Here, we conducted an I/I0 analysis and added some clarifying language about the possible nature of line broadening in these samples. See new Figure S12 and Lines 268-274.

> *(6) Line 126 "Importantly, many resonances are also minimally impacted." This statement is unclear since from the plots shown in Figure 1D, it seems that many of the residues are impacted by RNA titration, see the point about differential broadening above, this sort of plot may help pick apart residues that broaden due to RNA contacts (rather than changing rotational correlation).*

We have removed this statement, in addition to our revisions above regarding the line broadening.

> *(7) Line 137 - I am not sure that a max chemical shift of 0.15 ppm constitutes "strong chemical shift perturbations"*

The Reviewer makes a good point. We have changed "strong" to "significant" which refers to 1 standard deviation above the 10% trimmed mean of the data. See Line 237.

> *(8) Line 144 - change to "...experimentally determined structure...".*

We have added new lines 135-136 to make this point clear. We reinforced that initial predictions were based on the Alphafold2, since an experimental structure was lacking, but we have now discussed the mutations in context of the new structural data.

> *(9) The section from lines 150 - 166, comparison of the effect of different mutations in different Cas9 seems more appropriate for the discussion section.*

We have added additional text on this point in the Discussion section, within several new paragraphs.

> *(10) In Figure S6, chemical shifts are observed at the distal site away from the mutations, could the authors discuss?*

The Reviewer makes an important observation. Indeed, the CSPs caused by K267E and R332A extend beyond the mutation site. These shifts are mostly close in 3D space to the mutation, and consistent in Figures 2 and S5. New titrations of gRNA into isolated *Geo*Rec2 also activate some distal sites, and new MD simulations suggests the mutations disrupt RNA and DNA contacts, where these distal effects may play a role with full-length gRNAs.

We agree it would be worth mutating distal sites undergoing CSPs to examine their impact on function, but two complicating factors are 1) the lack of substantial gRNA affinity differences in experiments with full-length *Geo*Cas9 and 2) the lack of functional changes in the mutants. In this initial study, it appears difficult to assign an effect to these distal sites in *Geo*Cas9 (beyond speculation). We do have a brief discussion of the distal sites (Lines 293-298) and will follow up this work with more comprehensive mutagenesis studies of these sites.

> *(11) It appears that the authors fitted the Tm data to some model although this is not mentioned in the text, figure captions, or methods. In the caption for Figure 4D the authors refer to "Fitted thermal denaturation profiles...".*

We have added the relevant Equation in the Methods and referenced it in Figure S6 and S14 captions.

> *(12) Details of the ModelFree fitting are needed, how many residues fit with the minimal models, and how many invoked Rex and other terms? How does the statement in line 191 about the elevated S2 values arising from global tumbling compare with an experimental estimation of rotational correlation eg. from R2/R1 ratios?*

We have included an expanded description of the Model-free protocol (Lines 521-527). The best diffusion tensor was an ellipsoid model. The number of residues utilizing Rex was 81, though Rex contribution was very small. The mean and errors for the fast motion (S^2_f), slow motion (S^2_z) and generalized order parameter were 0.97 ± 0.15, 0.84 ± 0.14, and 0.91 ± 0.20, respectively.

R2/R1 ratios for each of the samples (relaxation conducted on *Geo*Rec2 in isolation) corresponded to an estimated tc of 16.3 ns for all data sets. This value is a bit larger than would be expected for a compact globular protein of 25 kDa, though our X-ray structure of *Geo*Rec2 shows a somewhat elongated domain.

> *(13) Line 221 - referring to two different figures at the end of the sentence is confusing, maybe place the figure references immediately after the referral in the sentence.*

We have resolved due to reshuffling of the Figures.

> *(14) Line 234 - Fig 4E is mentioned before fig 4D, in fact Fig 4D is not mentioned in the text.*

We have reordered and edited many of the Figures, this is now resolved.

> *(15) Line 243 - what is the saturating concentration to which the authors are referring?*

We have amended the Results section to more clearly discuss the effect of gRNA on the *Geo*Rec and (now) *Geo*Rec2 domains. We meant 3-fold excess gRNA-to-protein by “saturating” in the prior version. At that point, CSPs held stable and the degree of line broadening at certain sites had completely obscured the resonance from view.

> *(16) Fig 4E caption - mentions error of 1.34 while the figure is labeled 1.1 for the R332A GeoRec mutant.*

This has been resolved due to additional MST trails as well as the editing and reordering of many Figures.

> *(17) Line 253 - the authors are discussing regions of allosteric hotspots, how do the motions of these predicted hotspots compare with the relaxation dispersion data? There seems to be some overlap.*

The Reviewer makes a keen observation. Yes, there is overlap in these data. For example, hotspot residue R269 is bracketed by L268 and L270 with relaxation dispersion. Also, hotspot L279 surrounded by C275, A276, R277, and D281 with dispersion in both variants. Further, D403 and E408 reside in a stretch of ms timescale flexibility comprised of N404, L406, N412, and L413. We have yet to fully understand the functional significance of this overlap, but have added a note in Line 298 to draw the reader's attention to it.

> ***Reviewer #3 (Recommendations For The Authors):***
>
> *Although the scope of the manuscript is rather limited due to the minor effects observed for the selected mutations, it is clear that a lot of work was done in spearheading the investigation of dynamic modes in GeoCas9 Rec2. In my view, the data will still be of relevance and interest to the general structural and chemical biology communities.*
>
> *However, there are a few technical shortcomings that need to be addressed and some statements that are poorly supported by data, necessitating either more experimental proofs or rephrasing of the conclusions.*
>
> *Major points:*
>
> *X-ray structure - No PDB ID, structural statistics, or validation report is given for the structure, so it is impossible to judge of the quality. Please provide these. Furthermore, it would be commendable to determine the structure of the point mutant Rec2 domains, this would greatly strengthen the claim that mutations affect only dynamics and do not change structure.*

We apologize for this oversight. We absolutely had these data at the time of submission but must have forgotten to upload them. The validation report is now attached.

Regarding the mutant structures, the Reviewer's point is well taken. In the absence of these structures, we have adjusted the language to include the possibility of structural change. We have also included new MD simulations (new Figure 6 and associated text) that provide comment on possible structural and dynamic changes due to mutation. We note that NMR spectral changes are quite modest, beyond the site of mutation. Further, the new binding data with full-length *Geo*Cas9 (new Figure 7) shows very little change in gRNA affinity with mutations, implying that a profound structural rearrangement does not take place.

> *Translating isolated Rec2 findings to FL GeoCas9 - This is an important point and I do appreciate that the authors discuss this. I agree that working on FL samples for NMR would not be feasible, but I am not convinced by the statement that "GeoRec2 in isolation represents the structure of the subdomain within full-length GeoCas9 very well". The chemical shift perturbations observed between isolated Rec2 and FL Cas9 are relatively sizable. This should be discussed in further detail. Figure 1B should showcase peaks having the highest perturbations. Are they located at termini or interaction interfaces?*

We have provided the combined ^{1}H-^{15}N combined CSPs for each construct, relative to the full-length *Geo*Rec domain, Author response image 1. In most cases, the largest CSPs occur at resonances on the periphery of the spectra, retaining the ability to unambiguously assign it. The largest CSPs do appear to exist at the termini.

The Rec1 and Rec2 subdomains are connected by a short, but flexible unstructured linker in full-length *Geo*Rec. Thus, the two subdomains do not form a particularly tight non-covalent interface and behave somewhat independently (see Figure S4, for example).

Regarding the statement of "*Geo*Rec2 in isolation...," we apologize for this confusion.

We were referring to our solved crystal structure in relation to the AlphaFold model. With the new cryo-EM structure of *Geo*Cas9 having been recently published, our X-ray structure of *Geo*Rec2 is still in excellent agreement, but we have clarified our intent on Line 111.

> *Dynamics and effect of mutations - K267E is more destabilizing and leads to more spread chemical shift perturbations throughout Rec2 and to faster-correlated dynamics but not in significantly lower affinity or cleavage. How do the authors explain this?*

The Reviewer raises an interesting question. Regarding the impact of the K267E mutation, new MD simulations also suggest K267E to be quite disruptive of the *Geo*Cas9 structure and dynamics, modulating contacts with the nucleic acids. However, further MD analysis of the recently published (*bona fide* high specificity) i*Geo*Cas9 variant shows that K267E only imparts a portion of the effect of i*Geo*Cas9, suggesting that even further modulation of *Geo*Rec would be require for substantial functional impact. In addition, new MST binding studies with full-length variants and gRNAs show K267E does not dramatically alter gRNA binding, suggesting that the lack of functional impact, despite biophysical change, is suppressed by the surrounding *Geo*Cas9 domains. We comment on this in the Discussion.

> *Moreover, the time regime for the fit of the CPMG curves is surprisingly slow given the profiles, how were the minor state populations? Were the dynamics really correlated? Please provide numbers (also see minor points below). In that regime CEST experiments should work, was that done?*

The minor state populations were very low in the analysis, <1%.

To examine the correlated dynamics, we compared the global fits to those of the individual fits for each residue and found them to be better for the global fit, based on the Akaike Information Criterion. For WT, the AIC showed the global fit to be ~10-fold better. For K267E, the global model was 4-fold better, and for R332A, the global model was 6-fold better. We have added language clarifying the use of AIC to the Methods section.

We have done CEST experiments on _Geo_HNH (we did not see overly clear evidence for a minor state), but we did not perform these experiments on *Geo*Rec. However, we strongly agree that a detailed follow-up study focusing on CEST and new *Geo*Rec variants should investigate this further.

Since the binding effects with gRNAs differ in the isolated domain and the full-length protein, we have tried not to over-analyze the impact of the relaxation data in this specific context. These data still provide useful information regarding the impact of point mutants on *Geo*Cas9 domain biophysics, and MD simulations support the enhanced dynamics seen in CPMG and other relaxation data. However, the functional implication is clearly more complicated and requires further study.

> *Mutations affect gRNA affinity - I am not convinced that affinity itself is significantly affected based on the MST data. This data could be reproduced as technical replicates to reduce the error bars, or another technique with less intrinsic noise (ITC, SPR) could be used to better support this claim. However, a 3-fold difference seen from NMR titrations could indicate a change in binding mode, for instance in koff. It would be interesting to obtain SPR or BLI data quantifying the kinetics of the interactions. Anyhow, this point should be more carefully discussed.*

We agree with the Reviewer on this point. We conducted additional replicates of MST trials, as well as new MST with a different gRNA sequence. Our updated analysis, including statistics, provides a better measure for "significance" in these data, which is now reported. We have also added some text discussing a possible change in binding mode, see Lines 256-259.

We also carried out MST on full-length *Geo*Cas9 with full-length gRNAs (the same two RNAs used as truncated constructs). We report these data in new Figure 7 and note there is essentially no difference between the gRNAs or the *Geo*Cas9 variants under these conditions.

Further, MD simulations suggest a change in binding energy associated with the gRNA interaction in the context of full-length *Geo*Cas9. Since experimental studies are not able to parse these differences, collectively, we describe a scenario where the highly stable structure of *Geo*Cas9 resists substantial mutation-induced change seen for analogous perturbations in *Sp*Cas9. See Lines 309-342, 414-418, and 448-461.

> *Minor points:*
>
> *• Please detail how the error on R1 and R2 rates was calculated.*

We have included new text in Lines 514-518.

> *• Please detail how hetNOE values were calculated (simply Isat/Iref?) and what values were used for Model Free.*

Yes, the Reviewer is correct. We have added specifically that we used Isat/Iref on Line 518.

> *• Please elaborate on the Model Free analysis. What tensor was used for tumbling? What was the correlation time? This is needed to judge the trustworthiness of S2 parameters.*

We have included new text on Lines 520-526. The diffusion tensor used was an ellipsoid and the correlation time was 15.4 ns. The correlation time estimated from R2/R1 ratios was 16.3 ns.

> *• Figure 1: Please indicate where Rec1 and Rec2 are located on panel A and indicate the residue assignments for each peak showcased in panel B.*

We have indicated the boundary of Rec1 and Rec2 in the new cartoon of Figure 1A. We have also noted the exact amino acids used for each construct in the Methods. We also added resonance labels to the spectral overlays in Figure 1B. We have done the same

> *• Line 187: I believe this should refer to Figure S8C rather than Figure 3A.*

We have made this change.

> • *Some fits of the CPMG curves look strange, e.g. R343 in Fig. 3B WT definitely does not contain significant us-ms dynamics and should be excluded from the analysis. Please double-check each profile. Were other models besides CR72 not providing better fits?*

The Reviewer has made a very careful observation. Our intent was to highlight these sites on purpose to show differences in CPMG relaxation dispersion between WT and variant samples. This was provided as some evidence for the redistribution of dynamics between samples, as many different sites found to be "rigid" on the ms timescale in WT *Geo*Rec2 were flexible in *Geo*Rec2 variants. We agree, however, that this Figure panel was confusing and have therefore removed it in favor of simple discussion in the text.

> • *To what degree are the CPMG dynamics correlated, can you provide statistical measures for the global fits?*

We compared the global fits to those of the individual fits for each residue and found them to be better for the global fit, based on the Akaike Information Criterion. For WT, the AIC showed the global fit to be ~10-fold better. For K267E, the global model was 4fold better, and for R332A, the global model was 6-fold better.

We have added language clarifying the use of AIC to the Methods section.

> • *Error measured from replicates and p-values should be reported for DNA cleavage assays.*

We thank the Reviewer for pointing out this omission. We have included error bars on these plots.

https://doi.org/10.7554/eLife.99275.2.sa0